Planetary Nebula Velocities in the Disk and Bulge of M31

C. Halliday[1,2,3,4], D. Carter[1], T.J. Bridges[5,6], Z.C. Jackson[1], M.I. Wilkinson[7],
D.P. Quinn [7], N.W. Evans[7], N.G. Douglas[8], H.R. Merrett[9], M.R. Merrifield[9],
A.J. Romanowsky[10], K. Kuijken[8,11], M.J. Irwin[7].

[1] *Astrophysics Research Institute, Liverpool John Moores University, Twelve Quays House, Egerton Wharf, Birkenhead CH41 1LD, UK.*
[2] *INAF - Osservatorio Astronomico di Padova, Vicolo dell'Osservatorio 5, I-35122 Padova, Italy.*
[3] *Institut für Astrophysik, Friedrich-Hund-Platz 1, 37077 Göttingen, Germany.*
[4] *INAF - Osservatorio Astrofisico di Arcetri, Largo E. Fermi 5, I-50125, Firenze, Italy.*
[5] *Anglo-Australian Observatory, PO Box 296, Epping NSW 1710, Australia.*
[6] *Department of Physics, Queen's University, Kingston, Ontario, K7L 3N6, Canada.*
[7] *Institute of Astronomy, Madingley Road, Cambridge CB3 OHA, UK.*
[8] *Kapteyn Astronomical Institute, Postbus 800, 9700 AV Groningen, The Netherlands.*
[9] *School of Physics and Astronomy, University of Nottingham, University Park, Nottingham, NG7 2RD, UK.*
[10] *Departamento de Física, Universidad de Concepción, Casilla 160-C, Concepción, Chile.*
[11] *Leiden Observatory, P.O. Box 9513, NL-2300 RA Leiden, The Netherlands.*

ABSTRACT

We present radial velocities for a sample of 723 planetary nebulae (PNe) in the disk and bulge of M31, measured using the WYFFOS fibre spectrograph on the William Herschel telescope. Velocities are determined using the [OIII]λ5007 emission line. Rotation and velocity dispersion are measured to a radius of 50 arcminutes (11.5 kpc), the first stellar rotation curve and velocity dispersion profile for M31 to such a radius. Our kinematics are consistent with rotational support at radii well beyond the bulge effective radius of 1.4kpc, although our data beyond a radius of 5kpc are limited. We present tentative evidence for kinematic substructure in the bulge of M31 to be studied fully in a later work. This paper is part of an ongoing project to constrain the total mass, mass distribution and velocity anisotropy of the disk, bulge and halo of M31.

Key words: galaxies: spiral; galaxies: individual – M31; galaxies: haloes.

1 INTRODUCTION

The Andromeda Galaxy M31 is our closest giant galaxy of any type, and presents the best opportunity for conducting a robust analysis of the dynamics of a galaxy disk, bulge and halo. Early studies of the kinematics of this galaxy were based upon the HI 21cm line velocities as a measure of rotation (Kent, 1989; Roberts & Whitehurst, 1975) and HII emission line regions (Rubin & Ford, 1970). Using a combination of the rotation curve measures, and kinematics of the bulge component as measured from radial velocities of 149 globular clusters, and assuming velocity isotropy, Kent *et al.* (1989) constrained the relative mass fractions of the disk and bulge of M31.

The extremely rapid rotation seen in integrated stellar light velocity measurements in the centre (Kormendy 1988; Carter & Jenkins 1993; van der Marel *et al.* 1994; Kormendy & Bender 1999) and the double nucleus seen in HST images (Lauer *et al.* 1993) have been interpreted as evidence for a central black hole of $1 - 3 \times 10^8 M_\odot$ (Bender *et al.* 2005). Models with a single rapidly rotating disk (Kormendy & Bender 1999) or two nested disks (Bender *et al.* 2005) have been proposed. The nucleus of M31 is clearly complex.

Due to the steep decline in radial surface brightness profiles of the galaxy integrated light, alternative probes of the galaxy mass distribution must be used at radii much greater than the bulge effective radius of 1.4 kpc (Pritchet & van den Bergh 1994; Irwin *et al.* 2005). The most recent HI 21cm observations of M31 are summarised by Braun (1991), who concludes that the rotation curve is well fitted by a mass distribution which follows the stellar light with a fixed M/L of 6.5 solar in the B band. He finds no need for a massive dark halo to a radius of at least 28 kpc. Nevertheless, spiral galaxies are widely believed to be dark-matter dominated in their outer parts, both to understand the majority of HI rotation curves, and to stabilise the disks (e.g. Ostriker, Peebles & Yahil 1974).

Ideal probes of the mass distribution should trace the kinematics of the galaxy disk, bulge and halo. With sufficiently large samples of kinematic measurements of these, it is possible to reconstruct the potential of a galaxy, and the distribution function of the tracer population for a spherical system (Merritt & Saha 1993; Merritt 1993), or an axisymmetric two-integral galaxy viewed edge-on (Merritt 1996). Whilst

neither of these approximations applies exactly to M31 (it is neither spherical nor edge-on), it is still possible to use discrete velocities to constrain self-consistent multi-component models (e.g. Widrow & Dubinski 2005).

Knowledge of the total mass of M31 is vital for the interpretation of the latest generation of pixel microlensing experiments, which concentrate on that galaxy (Crotts 1992; Kerins *et al.* 2001, 2003; de Jong *et al* 2004; Cseresnjes *et al.* 2005; Riffeser *et al.* 2003; Belokurov *et al.* 2005). Evans & Wilkinson (2000) have found that there is no kinematic evidence to support the widely-held belief that M31 is more massive than the Milky Way, in contradiction to previous studies. Their measurement is uncertain by a factor of ∼2, the main source of uncertainty being the small number of available tracer velocities particularly at large radii. Evans *et al.* (2000) presented radial velocity measurements for the 15 dwarf companions known at present, and derived a total mass of M31 in the range $7 - 10 \times 10^{11} M_\odot$.

Globular clusters have the advantage of being found at large galactocentric radii, but they are not present in large numbers in spiral galaxies. Perrett *et al.* (2002) presented radial velocities for 202 globular clusters, mostly along the disk of M31. Kent *et al.* (1989) and Huchra *et al.* (1991) presented 149 globular cluster radial velocities, including some from older sources. Smaller samples are presented by Federici *et al.* (1993; 35 globular clusters), and Jablonka *et al.* (1998; 16 clusters). With some duplication, the total sample of globular cluster velocities is now of order 300. Evans *et al.* (2003) combine the globular cluster velocities from Perrett *et al.* with the dwarf satellite velocities, and deduce that M31 has a dark halo which is isothermal out to at least 100 kpc, and has a total mass within that radius of $\sim 1.2 \times 10^{12} M_\odot$.

Planetary nebulae (PNe) are not as spatially extended as globular clusters. They are readily detectable however due to their bright [OIII] emission lines, and are substantially more numerous than globular clusters. Their spatial distribution in M31 is expected to reflect that of the old stellar population of the disk and bulge. Pritchet & van den Bergh (1994) find that the distribution of the bulge stellar population can be fit by a single de Vaucouleurs (1948) law from the inner bulge at a radius of 200 parsecs, out to ≈20 kpc, beyond which the profile flattens to an exponential or a power law of index about -2.3 (Irwin *et al.* 2005). PNe are used as tracers of galaxy kinematics using two different methods: PNe are identified in narrow band, wide field [OIII] images, and then their velocities measured subsequently with a multi-object spectrograph (e.g Arnaboldi *et al.* 1996; Arnaboldi *et al.* 1998; Hui *et al.* 1995; Peng *et al.* 2004); or a slitless spectrograph combined with narrow-band filters is used to complete imaging and spectroscopy in a single observation, albeit with a narrower field of view (Douglas *et al.* 2000, 2002; Méndez *et al.* 2001).

Hurley-Keller *et al.* (2004, hereafter HK04) present radial velocities of a sample of 135 PNe to the South and East of the nucleus of M31. They find that most of the PNe in their sample belong to rotationally supported disk and bulge components, with no evidence for a dynamically hot halo, although the sample of PNe they have studied is rather small.

Here we present accurate velocities for 723 PNe observed using the first of these two approaches, using the WYFFOS multi-object spectrograph on the William Herschel Telescope on La Palma. In section 2.1 we describe methodology for object selection and astrometry; in section 2.2 we describe the spectroscopic observations and basic data reduction; in section 2.3 we outline our measurement of PNe radial velocities and determination of velocity errors. In section 3 we present a kinematic analysis of the disk and bulge of M31. A survey of a larger number of PNe has been completed using the Planetary Nebula Spectrograph (Douglas *et al.* 2002). Using a subsample of these velocities, Merrett et al. (2003) trace the kinematics of the southern stellar stream of M31 through the body of the galaxy, and suggest a possible stream orbit. The complete velocity dataset from the Planetary Nebula Spectrograph, together with a detailed comparison with the current dataset will be presented by Merrett *et al.* (2006). A further paper will present a detailed astrophysical analysis of the joint dataset.

2   OBSERVATIONS AND DATA REDUCTION

2.1   Sample and Astrometry

Our spectroscopic data were acquired during two observing runs at the William Herschel Telescope, in August/September 1999 and in October 2001. Between our spectroscopic runs we completed an [OIII]+ Strömgren y imaging survey using the Isaac Newon Telescope to detect additional PNe targets out to a projected radius of 20kpc. Here and throughout this paper we assume a distance of 770 kpc for M31. The sample selection and astrometry thus differed between the 1999 and 2001 runs, and we describe each in turn.

The 1999 sample is derived from an original sample of 429 PNe detected by Ciardullo *et al.* (1989) (hereafter C89) from [OIII] and continuum images of M31 taken in an irregularly shaped region approximately 33 x 3 arcminutes in the disk of M31. C89 quote positions for equinox and epoch B1975 and the internal precision of the positions is good. In a successful multi-fibre observing run the telescope is aligned on the target field using bright fiducial stars since the PNe are not visible to an acquisition camera. The purpose of our astrometric procedure was to ensure that our PNe targets and fiducial stars were on a common system, aligned with the International Celestial Reference Frame.

The raw material for our astrometric solutions were archive images from the INT Wide Field Survey (WFS), particularly V band images of two fields studied for the INT M31 pixel microlensing project. Each exposure was 599 seconds in V for the four separate CCDs of the INT Wide Field Camera (WFC).

It was first necessary to set up a secondary astrometric reference grid on the WFC CCD images. This was completed using Digital Sky Survey[1] (DSS) images. A sample of 42 primary astrometric standards was chosen from the PPM catalogue (Monet *et al.* 1996). Using catalogued positions and positions measured on the frame, an astrometric solution for the DSS image was derived using the Starlink[2]/AAO

---

astrometric transformation programme `ASTROM`, written by P.T. Wallace. Positions of secondary standards were then measured from the DSS images, and transformed to the primary astrometric reference frame.

The astrometric solutions were derived from the secondary standards. Between 35 and 40 secondary standards were measured on each of the four CCD images in each of the two WFC fields of M31. Using these standards, again using `ASTROM`, and using a model of the geometrical distortion at the prime focus of the INT provided by R.W. Argyle, an astrometric solution was derived for each CCD image.

Because the WFC images were continuum the majority of the PNe were not visible on them, but the brightest few were. The C89 positions are derived from a set of reference stars given in Ford and Jacoby (1978) (FJ78). To transform the C89 positions to our reference frame we assumed that they were measured correctly with respect to the FJ78 standards, and measured the offset between the FJ78 positions precessed to J2000, and our measured J2000 positions of the FJ78 stars. These offsets were of order 1 arcsecond in RA and Dec, with a scatter of 0.4 arcsec. The consistency of the procedure was checked by measuring 4 bright PNe in the C89 sample on the WFC frames.

Our catalogue for the 1999 run comprises the C89 catalogue precessed to J2000, and with the offset derived above applied, together with measured positions of fiducial stars suitable for use with WYFFOS.

For the 2001 sample both the PNe and fiducial star positions were determined from a set of [OIII] narrow band and Strömgren y continuum images obtained between August 3rd and 8th 2000 with the INT Wide Wield Camera (WFC). The Strömgren y filter defines a convenient continuum band close in wavelength to, but not containing, the [OIII] lines. A list of 1284 potential targets was drawn from 12 sets of WFC images, covering a field of approximately 1.6 degrees in Declination (Dec) by 1.4 degrees in Right Ascension (RA), centred on M31. Each set consisted of three 1200 second exposures in [OIII] and three 300 second exposures in Strömgren y. After reduction some of these images were rejected because of problems with image quality, so the depth of the images was not uniform from field to field. Remaining images were bias subtracted, flatfielded and coadded, to provide one deep frame in each passband. Corresponding coadded [OIII] and Stromgren y images were then compared visually using the blink function of the Starlink `GAIA` image display package. PNe were identified as objects appearing in the [OIII] frame but not the Strömgren y frame, and their pixel co-ordinates were measured using the centroiding algorithm of the aperture photometry function of `GAIA`. Positions of fiducial stars were measured from the [OIII] frames in the same way.

Pixel co-ordinates were then transformed to ICRF J2000 RA and Dec using the same procedures as for our 1999 dataset. A set of secondary standards was set up on each WFC CCD image using a DSS image, and the positions of the PNe and fiducials were calculated from these secondary standards, each time using `ASTROM`. Our final positions of PNe and fiducials have a relative precision of around 0.4 arcseconds, although the absolute accuracy of our astrometric frame is around 1 arcseconds. Merrett *et al.* (2006) present a comparison of the astrometry from this paper with that derived independently from PN.S data. They find that the combined error $\sigma = (\sigma_{PNS}^2 + \sigma_{H06}^2)^{1/2} = 0.48$ arcsec in RA, where H06 refers to the current paper, with a lower dispersion in Dec but with a systematic offset of 1 arcsecond between the positions in the central fields. This offset could be in either dataset.

From the positions of the PNe which were successfully observed in both runs, we find that the 1999 and 2001 co-ordinate frames are consistent, the formal offset is that the 1999 positions are 0.03±0.02 seconds of time lower in RA, and 0.1±0.1 arcseconds higher in Dec, than the 2001 positions. Considering the offset between the C89 positions, transformed to J2000, and the 2001 positions we find that the offset is dependent upon position in the field. Over that part of the field covered by the FJ78 secondary standards, the C89 positions again are consistent with ours, formally the C89 positions are 0.02±0.01 seconds of time lower in RA, and 0.1±0.1 arcsec higher in Dec than our 2001 positions. However C89 note that their positions are less reliable in the NE fields not covered by FJ78 secondary standards, and in these fields we find that C89 positions are 0.13±0.04 seconds of time higher in RA, and 1.2±0.2 arcseconds higher in Dec than our 2001 positions (i.e. an offset of about 1.5 arcseconds on the sky).

In order to reduce contamination of the sample by HII regions, extended objects were not selected. It is possible that some compact HII regions remain in the sample. Except at the brightest magnitudes it is not possible to separate HII regions from PNe using narrow band imaging alone (Merrett *et al.* 2006), and this would only be possible using flux calibrated spectra with a wide wavelength range.

In table 1 we present the positions of a representative subset of the fiducial stars in the astrometric system of this paper. These positions could be used for fiducials for future fibre spectrograph runs, or as tertiary standards for astrometry of further objects in the M31 field. Our full astrometric database of 1284 PNe positions, and 313 potential fiducial stars, is available in tabular form from either of the first two authors.

2.2 Spectroscopic Data and Reduction

Spectra were obtained of PNe targets in two separate spectroscopic runs with the WYFFOS fibre fed spectrograph (Worswick *et al.* 1995) on the William Herschel Telescope. WYFFOS was fed from the AutoFib 2 robotic fibre positioner (Parry *et al.* 1994). Targets were selected to maximize the number of objects observed using the configuration program `AF2_configure`. The minimum object to object spacing of 25 arcseconds means that towards the centre of M31 many objects cannot be observed. There is however no lack of targets in the central region.

Our wavelength range of ∼350Å was centred on the [OIII]λ4959Å and [OIII]λ5007Å emission lines, using the WYFFOS echelle mode in 5th order. Four different 20 minute exposures were made consecutively for each configuration. Flat-field and neon comparison arc lamp exposures were obtained separately for each configuration.

On the nights of 30th August to 2nd September 1999 we observed 12 different WYFFOS fibre configurations based upon the input catalogue from C89, yielding a total of 294 PNe spectra. During this run we used the original "large" fibre module of WYFFOS, with 2.7 arcsecond fibres, and the consequent spectral resolution was 0.9 Å. Between 24th and 28th October 2001 we acquired data for a further 12 WYFFOS configuration to a radius of 11.5 kpc based on an input catalogue of 1284 PNe created from our INT WFC data. During this run we used the "small" fibre module of WYFFOS, with 1.6 arcsecond fibres, and the consequent spectral resolution was 0.5 Å. These data provided a further 482 PNe spectra. The efficiency of this run at detecting faint PNe was however lower, owing to the smaller fibre sky area.

Table 1. Positions of a representative selection of fiducial or tertiary astrometric standard stars

Identifier	RA (J2000)	Dec (J2000)
FD_12_2_9	0 38 1.350	40 49 24.38
FD_7_2_7	0 38 9.424	41 51 1.33
FD_7_4_8	0 38 36.612	42 2 34.67
FD_8_3_6	0 38 43.761	41 34 27.69
FD_7_3_4	0 38 44.420	42 4 11.44
FD_7_1_7	0 38 45.846	41 40 21.24
FD_12_3_1	0 38 47.375	41 5 1.19
FD_12_3_2	0 39 1.388	41 2 53.71
FD_12_4_2	0 39 11.011	40 46 8.65
FD_12_3_4	0 39 32.871	41 1 54.33
FD_12_3_6	0 40 4.205	41 4 17.88
FD_7_3_7	0 40 4.473	42 13 32.58
FD_11_1_2	0 40 57.999	41 43 52.33
FD_11_3_8	0 41 13.546	42 6 3.83
FD_6_2_3	0 42 2.068	41 13 51.53
FD_6_2_7	0 42 8.981	41 23 30.29
FD_6_2_2	0 42 20.216	41 7 46.82
FD_6_2_5	0 42 30.763	41 10 9.66
FD_11_4_7	0 42 35.463	41 57 46.87
FD_10_4_8	0 42 41.726	41 55 33.18
FD_6_3_1	0 43 1.609	41 30 7.62
FD_6_4_3	0 43 14.718	41 24 59.03
FD_6_1_2	0 43 32.620	41 9 9.31
FD_10_4_3	0 43 41.653	41 53 11.48
FD_5_2_10	0 43 46.899	41 26 11.35
FD_10_4_1	0 44 11.361	42 2 44.81
FD_9_2_5	0 44 22.363	41 54 0.15
FD_4_2_2	0 44 30.108	40 46 29.34
FD_6_1_3	0 44 30.574	41 15 37.17
FD_6_3_3	0 44 35.570	41 30 36.09
FD_4_1_1	0 44 47.807	40 34 22.34
FD_9_3_1	0 45 8.474	42 9 58.52
FD_9_1_8	0 45 34.204	41 41 43.99
FD_4_3_6	0 45 38.023	40 57 38.22
FD_5_4_8	0 45 43.785	41 19 43.98
FD_9_1_7	0 45 45.974	41 49 20.30
FD_4_3_2	0 45 46.630	40 56 47.39
FD_4_4_10	0 46 4.986	40 46 4.43
FD_4_4_9	0 46 9.054	40 51 14.29
FD_4_4_11	0 46 36.072	40 45 39.41

Data reduction was performed using the **wyfred** task of the **rgo** and **wyffos** packages in IRAF[3]. Aperture identification was completed using our flat-field CCD exposures. Wavelength calibration was performed to a typical accuracy of 0.003Å (0.2 km s^{-1} at 5000 km s^{-1}): this was achieved by fitting a polynomial of order 5-7 for the positions of 9-12 neon arc lamp spectral lines. To optimise the signal-to-noise ratio all exposures for a given configuration were median-combined to produce a single frame; this also allowed a larger number of spectra for fainter PNe to be studied. Examples of our PNe spectra are shown in Figure 1.

Spectra were not sky subtracted. Time was not scheduled to complete offset sky exposures during observations because sky-subtraction and flux calibration of spectra were not essential to complete our science goals.

2.3   Measurement of Planetary Nebulae Velocities

A velocity was determined for each planetary nebula (PN) by fitting a Gaussian function to the [OIII]λ5007 and, where visible, [OIII]λ4959 emission lines using a program provided by Dr. Bianca Poggianti (Dressler *et al.* 1999; Poggianti *et al.* 2006).

The central wavelength of each Gaussian was converted to a velocity using rest-frame wavelengths in air for the lines taken from the NIST[4] Atomic Spectra Database. Many of the detected emission lines had slightly square-topped profiles which could not be well fit by a
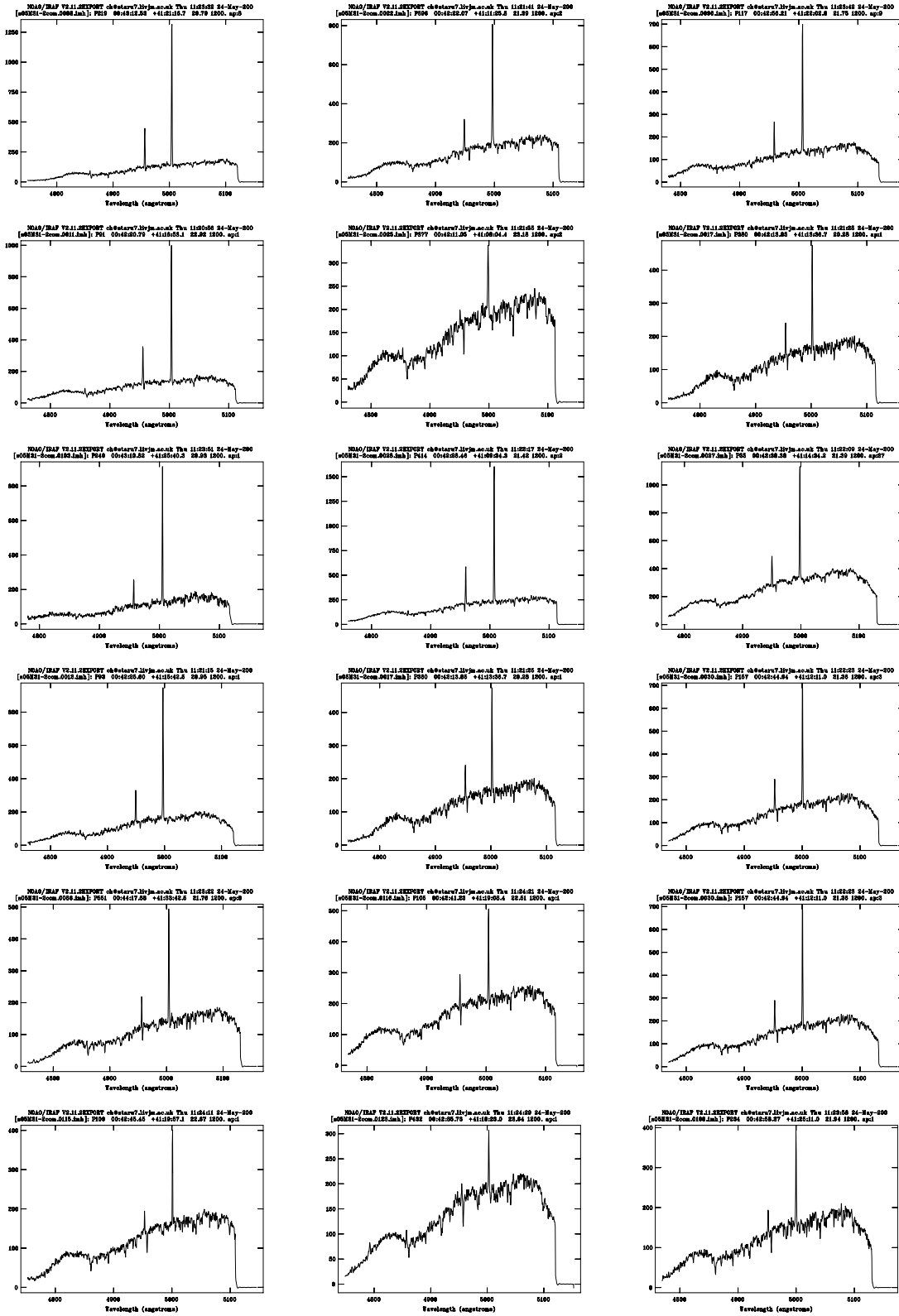

Figure 1. Typical PNe spectra for combined exposures of different WYFFOS configuration. Both [OIII] emission lines at 4959Å and 5007Å are visible for these spectra. The [OIII] 5007Å emission line wavelength is used to determine the planetary nebula velocity.
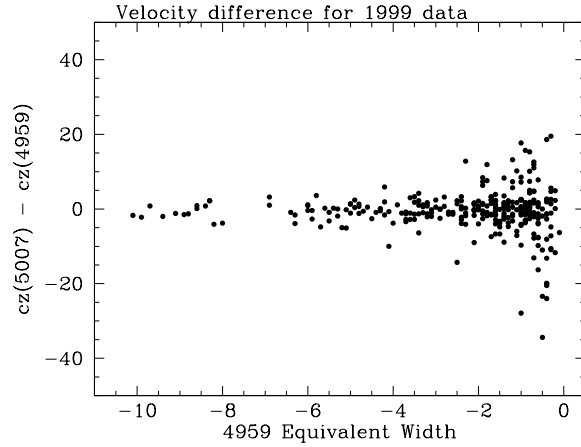
Figure 2. Difference between velocities calculated from λ5007 and λ4959, plotted against the strength of the weaker line, for the 1999 data.
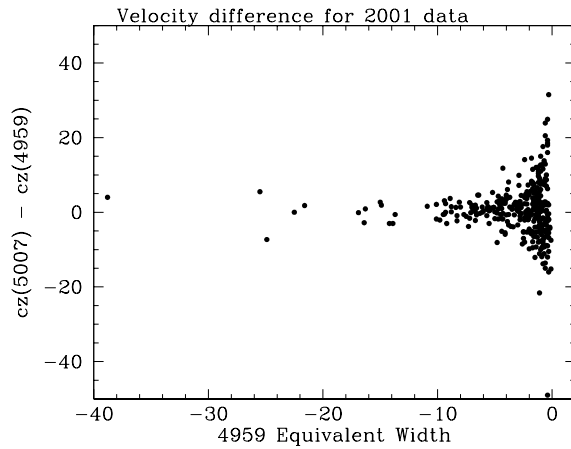
Figure 3. Difference between velocities calculated from λ5007 and λ4959, plotted against the strength of the weaker line, for the 2001 data.

Gaussian. To improve fitting each PN spectrum was convolved with a Gaussian of width 0.5 pixels; this smoothing had a negligible effect on the measurement of wavelength.

The [OIII]λ4959 line was used only in the estimation of the errors. This line is weaker than [OIII]λ5007 by a factor 3, and in addition is more affected by absorption lines in the sky background spectrum; as our spectra were taken in a mixture of grey and bright time the background is largely scattered solar light.

Velocities calculated from the wavelengths of the [OIII] lines were corrected to heliocentric using corrections calculated using the Starlink program rv. Internal velocity errors were estimated by comparing the velocities measured with [OIII]λ4959 and [OIII]λ5007 lines. Each velocity measurement will have an error due to the error in the estimate of the centroid of the line, and a calibration error due to thermal or mechanical shifts between PNe and comparison lamp spectra, and systematic errors in wavelength fitting. The first will depend upon the strength of the line, and will affect the [OIII]λ4959 and [OIII]λ5007 velocity measurements independently, whereas we assume the second will not depend upon the strength of the lines, and will affect the [OIII]λ4959 and [OIII]λ5007 velocity measurements identically in an individual spectrum. We estimate the first from differences between the velocity measurements of the two lines in individual spectra, and the second by comparing velocities from repeat observations of PNe.

We parameterise the error measurements in terms of the detectability of the emission line, which we have chosen to quantify in terms of the ratio of the emission line strength to the background (sky + galaxy) continuum, as the spectra are not sky subtracted. For each [OIII] emission line, a measure of this ratio was made, which we express as an equivalent width (EW).

PNe were separated into five bins of EW measurement of the [OIII]λ4959 line. For PNe in the bin of the highest [OIII]λ4959 EW measurement, we calculated the rms difference between the velocities calculated from [OIII]λ4959 and [OIII]λ5007, and assumed that errors in the wavelengths of the two lines contributed equally to these differences. This gives a value of the centroiding error for the lines in the strongest bin. For weaker bins, we assume that the centroiding error on the [OIII]λ5007 line is the same as in the strongest bin, and obtain a somewhat conservative estimate of the centroiding error for [OIII]λ4959 lines in each strength bin. In figures 2 and 3 we plot the difference between the velocities measured from the two [OIII] lines against the "equivalent width", a measure of the strength of the [OIII]λ4959 line, for the 1999 and 2001 runs respectively.

Next we assume that the centroiding error on a [OIII]λ5007 line is the same as that on a [OIII]λ4959 line of the same "equivalent width". Thus we construct a table of errors on the velocities computed from the [OIII]λ5007 lines.

In each run there are a number of repeat measurements, for each pair of measurements we compute the difference. We then restrict the comparison to lines with [OIII]λ5007 in the top two bins by line strength (for which the centroiding errors are nearly equal). We assume that the rms velocity difference is composed of centroiding error on each spectrum, plus calibration error, added in quadrature. Thus we compute the calibration error.

The errors presented in Table A1 are the sum in quadrature of these two components. This analysis was carried out separately on 1999 and 2001 data. Both the centroiding and calibration errors were somewhat higher in 2001 – in the case of the centroiding error we believe this to be due to brighter sky conditions.

All duplicate observations were then combined, with weights calculated from the inverse variances, and a final error calculated from summing the inverse variances. Analysis of objects observed in both 1999 and 2001 showed that there was no systematic offset between the velocity systems of the two runs, and that the rms difference was consistent with the individual errors upon the measurements. At this point we noted one very discrepant object, which we discovered to be very close to edge of the frame in the 2001 data, and found that the calibration procedure had failed at the edge of this frame. This point, and points around it in the data frame, were then rejected from the dataset, and do not appear in the final table.

Our final velocities are listed in Table A1. In this table the first column gives an identifier; if it is listed by C89 their identifier is used (of the form Pxxx), otherwise it has an identifier from our imaging survey (PN_field_object). Columns 2 and 3 give the position in J2000 co-ordinates, column 4 and 5 the final heliocentric velocity and its error. Columns 6 and 7 give the distance from the nucleus along the major axis and minor axis respectively, where we have adopted the position of the nucleus listed in the NASA NED database, close to that given by Crane *et al.* (1992). We assume a major axis position angle of 38.1°. Column 8 gives the distance from the nucleus, again in arcminutes, and column 9 the azimuthal angle (measured through west from north) in degrees. Column 10 gives the number of observations combined to give the final velocity.

HK04 published a list of 135 PNe velocities in fields to the South and East of the centre of M31. Some of their area lies outside our survey area, but there are 42 targets in common. Comparison of these results with ours shows that there are two objects whose velocities are discrepant. For PN_5_1_3 (=HKPN121) we have detections of [OIII]λ5007 and [OIII]λ4959 at the same velocity; this is in the highest error bin of HK04, and we are confident that our velocity is correct. For PN_2_1_15 (=HKPN66) there is no clear reason for the discrepancy, but we do not see [OIII]λ4959 or Hβ, so this could be a misidentification of the line on our part.

Neglecting these discrepancies we find a mean velocity difference of 8.7 km/s, in the sense that the HK04 velocity system is positive with respect to ours, and an rms velocity difference of 10.2 km/s after subtracting the zero point difference, which is consistent with the quoted errors on the two datasets.

Merrett *et al.* (2006) measure velocities for almost all of our PNe, and find a systematic offset and trend, which they attribute to a systematic shift in the PNS wavelength calibration. After transforming their velocities to the system of the current paper, they find a combined error $\sigma = (\sigma_{PNS}^2 + \sigma_{H06}^2)^{1/2} = 15.4$ km/s. This is consistent with the errors quoted in the present paper, and the expectation for the mean errors in the PNS velocities.

In Figure 4 we show the positions of the PNe in our sample using a standard coordinate projection centred on M31. The ellipses overlaid in the plot represent the disk and a flattened halo.

3 KINEMATICS OF THE PN DATA SET

In this section we present a brief analysis of the kinematics of our PN data set. Full dynamical modelling of these data, along with a number of other new kinematic data sets in M31 will be presented elsewhere. In the following, we use the convention that the positive X-axis is along the receding side of the major axis of M31. The transformations between RA and Dec and (X, Y) are as given by Huchra *et al.* (1991). We assume that the centre of M31 is at (R.A., Dec.) = 00:42:44.324, +41:16:08.53 (J2000) and that the position angle of the major axis is 38.1° (Ferguson *et al.* 2002).

Figure 5 plots the velocities of our PNe versus their major axis position. From the Figure, it is clear that our data set is dominated by rotationally supported components, as would be expected given the spatial distribution of our targets, which mostly probe the disk and bulge of M31.

Simple geometric arguments imply that for a star with minor axis distance $|Y| < 0.5$kpc, the line of sight velocity is close to the azimuthal velocity. By considering stars close to the major axis we can therefore obtain a meaningful stellar rotation curve and line of sight velocity dispersion profile. The top panel of Figure 6 displays the velocities against major axis position for PNe with $|Y| < 0.5$kpc (or 2.23′). The middle and bottom panels of Figure 6 show the velocity and dispersion profiles that we determine from the data. In order to fit the velocity and dispersion profile we assume that at each point the underlying velocity distribution follows a Gaussian with mean velocity $\bar{v}(r)$ and dispersion $\sigma(r)$. We fold the data assuming a systemic velocity for M31 of -310km s^{-1} and construct radial bins containing 40 PNe [5] each with velocities v_i and corresponding measurement errors σ_i. The probability of obtaining the ensemble of observed velocities in a radial bin is:

$$P(\{v_i\}|\{\sigma_i\}, \bar{v}, \sigma) = \prod_i \frac{1}{\sqrt{2\pi(\sigma_i^2 + \sigma^2)}} \exp\left(-\frac{(v_i - \bar{v})^2}{2(\sigma_i^2 + \sigma^2)}\right) \tag{1}$$

---

[5] The outer bin contains 21 objects.
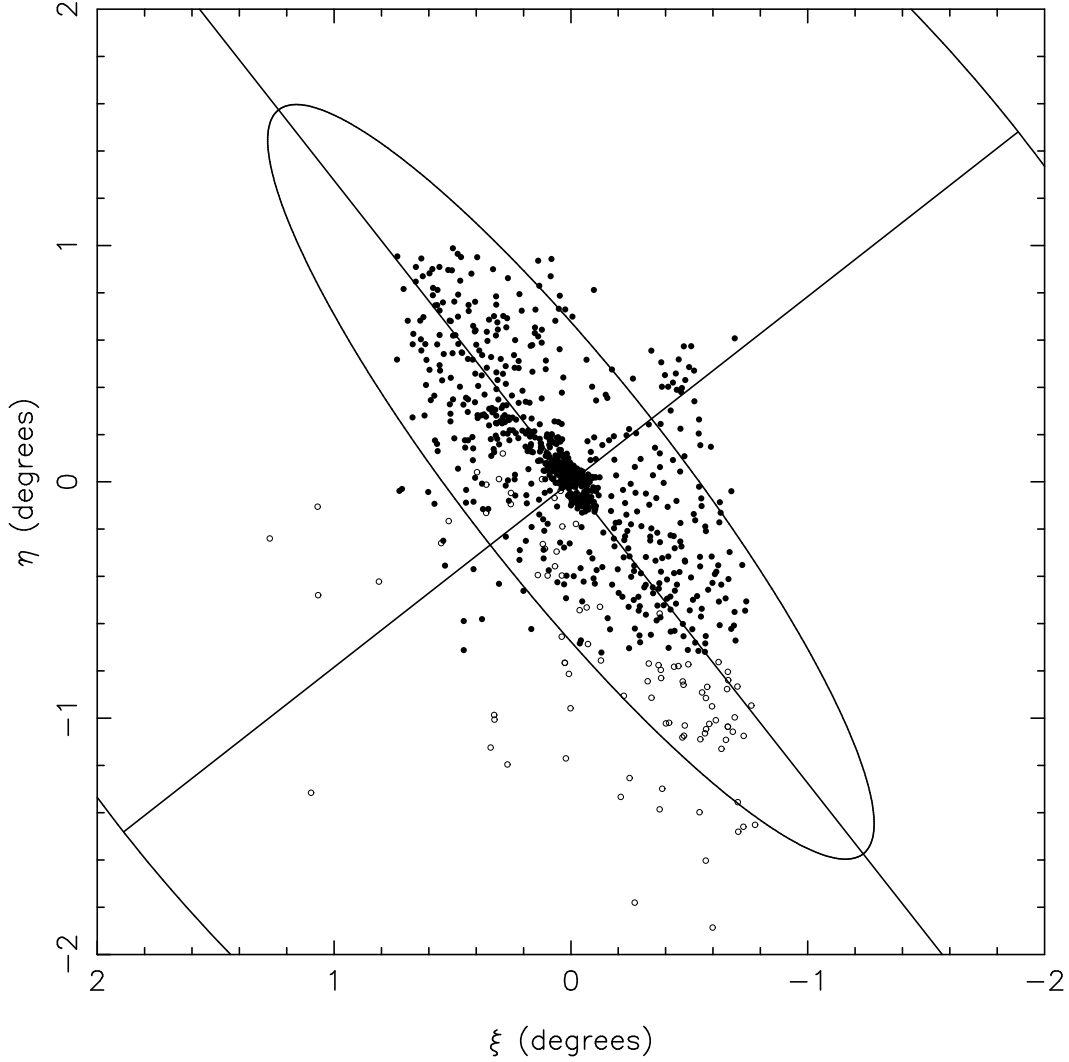
Figure 4. Positions of PNe with measured velocities, relative to the centre and orientation of M31. Filled symbols represent PNe from the present paper, open symbols PNe for HK04 which are not common with our sample. The inner and outer ellipses are drawn using a position angle of 38.1°. The outer ellipse represents a flattened ellipsoidal halo (aspect ratio 3:5) of semi-major axis radius 4° ($\approx$ 55 kpc). The inner ellipse has a semi-major axis of 2° ($\approx$ 27 kpc) and represents an inclined disk with $i = 77.5°$.

Table 2. Line of sight velocity and velocity dispersion data (plotted in Fig. 6). Columns give: (1) major axis position X in arcmin; (2) mean velocity in km s^{-1}; (3) miniumum and (4) maximum values of the mean velocity (1σ range); (5) velocity dispersion in km s^{-1}; (6) minimum and (7) maximum values of the velocity dispersion (1σ range); (8) number of stars in the bin.

X (arcmin)	$\bar{v}$	$\bar{v}_{min}$	$\bar{v}_{max}$	σ	σ_{min}	σ_{max}	N
1.15	35	13	58	135	122	155	40
2.79	54	33	75	125	113	144	39
5.34	94	71	117	140	126	161	40
8.52	138	121	155	98	88	114	38
21.00	196	184	209	69	62	81	38
46.81	202	193	212	50	45	59	33

Equation (1) is only strictly true within a bin if the rotation velocity is constant in the bin. In the inner zone where rotation velocity is varying rapidly as a function of radius the derived dispersion is artificially inflated by the variation of the rotation velocity. However this is not a large effect, as, for a uniform distribution within the bin, the dispersion is only inflated in quadrature by the bin velocity range divided by $\sqrt{12}$. For a velocity range of 50 km s^{-1}, this results in an increase in the dispersion of about 1 km s^{-1}.

For each radial bin we estimate $\bar{v}$ and σ by maximising the expression for the probability with respect to these parameters. We account for the effect of outliers by repeating the maximisation procedure twice. In the first iteration we omit PN data falling more than 2σ away from
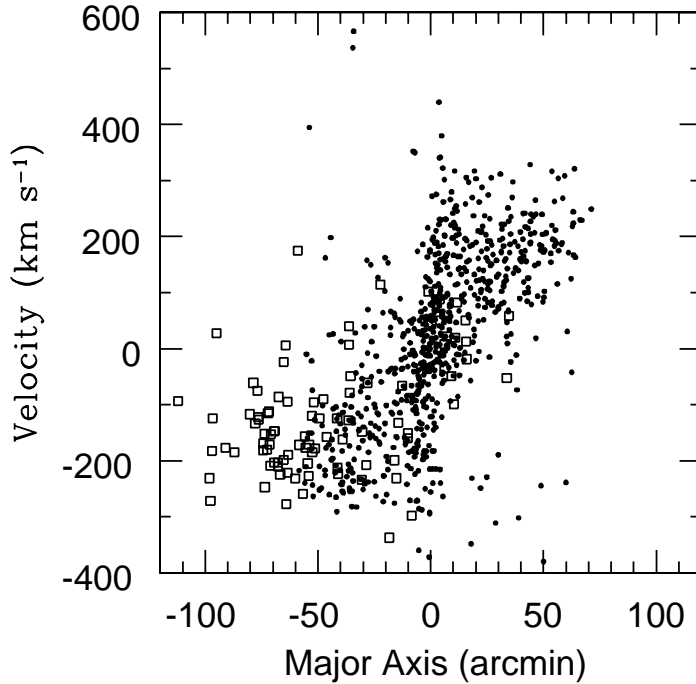
Figure 5. PN velocity versus distance along the major axis for our complete data set (solid symbols). The open squares denote those PNe observed by Hurley-Keller et al. (2004) which were not re-observed as part of our survey.

the mean velocity of the bin as defined by the initial fitted parameters. The second iteration uses a 3σ cut based on the updated parameters. The middle and bottom panels of Figure 6 show the results of this procedure, which are also tabulated in Table 2. The errorbars in each parameter shown in the plots are 1σ errors obtained by numerically determining the probability density function for that parameter by marginalising over the other parameter. We then define the 1σ confidence interval as the interval centred around the peak of the probability density function which contains 68 per cent of the probability. The systemic velocity used in folding the data is estimated using the complete data set from Figure 5. Using these data a rotation curve is calculated, as discussed above - the systemic velocity is then calculated by linear interpolation between the two bins on either side of the minor axis. In this way we obtain a value of $-310 km s^{-1}$ for the systemic velocity of M31.

It is clear from the top two panels of Figure 6 that the disk of M31 dominates the velocity distribution at these small distances from the major axis. The profiles in the two lower panels therefore constitute the first complete rotation curve and dispersion profile to 50 arcmin radius for the disk of M31 based on stellar kinematics. There have been many stellar kinematic studies in the very central regions, close to the black hole (e.g. van der Marel *et al.* 1994). At intermediate radii the most comprehensive study is by McElroy (1983), who presented long-slit velocity and velocity dispersion curves at several position angles, out to a maximum of 10 arcminutes radius. At larger radii, the data of HK04 were insufficient to determine the profiles of kinematic parameters. For comparison, in the middle panel we show the gas rotation curves of Braun (1991) and Kent (1989). Our PNe rotation curve is compatible with the curve of Kent (1989), however inside 30 arcminutes Braun's curve shows more rapid rotation than the PNe, and indeed than Kent's gas rotation curve. The differences between the two HI rotation curves are due largely to differences between the models used to turn observed gas velocity into circular speed. McElroy (1983) has also found the stellar velocity to be lower than the gas velocity, even after allowing for projection effects. The stellar rotation is expected to be lower than due to asymmetric drift (Gerssen *et al.* 2000), and possibly also to inclusion of thick disk and bulge components.

Following HK04, we illustrate the spatial variation of the velocity distribution in our sample by dividing our data according to minor axis distance (Figure 7). Projection effects make the velocity distributions at larger distances from the major axis more difficult to interpret. For $|Y| > 2.23'$ we expect to see a mixture of bulge and disk PNe (and potentially halo PNe also). Moreover there will be an apparent flattening of the rotation curve at large minor axis displacements even for the thin disk PNe, simply because of the projection of velocity and position in a tilted, thin disk with circular orbits. The upper panel of Figure 7 plots the data for $2.23' < |Y| < 26'$ (the optical edge of the disk projects to approximately $5.8 kpc$ or $26'$ along the minor axis). It is clear that the PNe in this sample are rotationally supported - the greater spread in velocities for a given X (compared to Figure 6) is due to the larger range of physical radii probed by these stars.

In the lower panel of Figure 7 we plot PNe with $Y < -26'$ as solid triangles, with the data with $|Y| < 2.23'$ also shown for comparison; we omit PNe with $Y > 26'$ as our sample in that region is dominated by likely members of the M31 satellite NGC 205 (based on their velocities and positions). The triangles in this plot show a similar trend to the data in the upper panel. This suggests that our data beyond the edge of the projected disk are still rotationally supported. This is consistent with the claim of HK04 that their sample of PNe outside 5.8kpc belong to an extended bulge rather than to a halo. Although our data at these large radii are clearly limited, no obvious signature of a hot, pressure-supported halo population is evident in the data set.

One of the main goals of kinematic studies of the disk and bulge regions of M31 is to establish the evolutionary history of the various components (see Morrison *et al.* 2004 for a detailed discussion). In this context, kinematic substructures are of particular interest as they
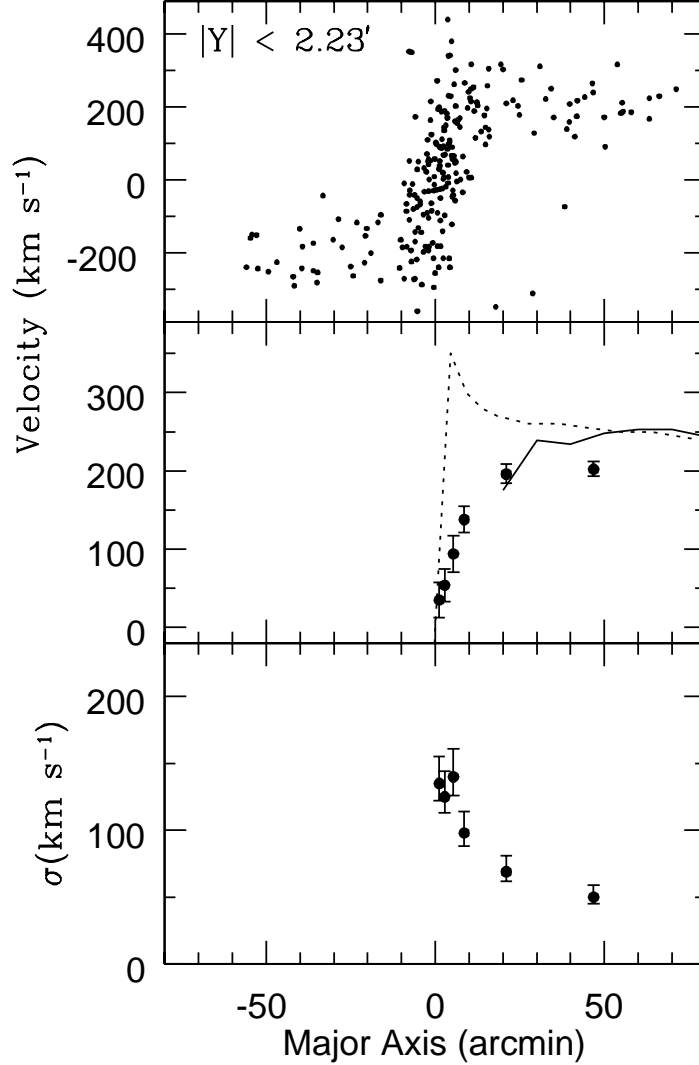
Figure 6. Line-of-sight velocity distribution for PNe with $|Y| < 2.23'$ (0.5 kpc). The top panel shows the PN velocity versus distance along the major axis. The middle and lower panels show, respectively, the mean velocity and velocity dispersion (with 1σ errors) as a function of major axis position. The sold curve in the middle panel is the gas rotation curve of Kent (1989) converted to line-of-sight velocity for comparison with our data; the broken curve is the rotation curve of Braun (1991). The data have been folded about the minor axis. See text for a detailed discussion.

may provide clues to the relative roles of mergers, accretions and in situ star formation. A number of recent studies have found evidence of substructure in M31, both kinematic and spatial (e.g. Ibata *et al.* 2001; Ibata *et al.* 2005; Merrett *et al.* 2003). In Figure 5 there are a number of conspicuous velocity outliers and in Figure 8 we show the spatial distribution of those PNe with $(X > 10', V < -150\mathrm{km\,s^{-1}})$ and $(X < -10', V > 100\mathrm{km\,s^{-1}})$ whose velocities imply that they are counter-rotating relative to the main disk population. We note that, based on their velocities and positions, the group of PNe located near $(-20, -20)$ are very likely to be associated with the satellite galaxy M32. Another group of PNe at $(5, 40)$ are likely associated with NGC 205. A third group of PNe in the vicinity of $(25, 0)$ appears to belong to a counter-rotating population that is not associated with a known satellite. These PNe have velocities consistent with possible membership of the giant southern stream (Ibata et al. 2001; 2004) since after traversing the nuclear region, the general symmetry of the potential field implies that far-side stream members will have similar velocities to those seen at the near-end of the stream on the south side of M31. Merrett *et al.* (2003) find a similar counter-rotating population of PNe, which appears to connect the southern stream to the northern spur, and five of the outliers in Figure 8 are common with their candidate stream extension objects. One or two groups of globular clusters were also found at this location by Perrett et al. (2003), reinforcing the identification of this component. It is also possible that the other small group of outliers with $X < 0, Y > 0$ could be part of the stream detached on a previous passage. We will investigate further possible substructure in the context of a complete dynamical model of M31 in a later paper.
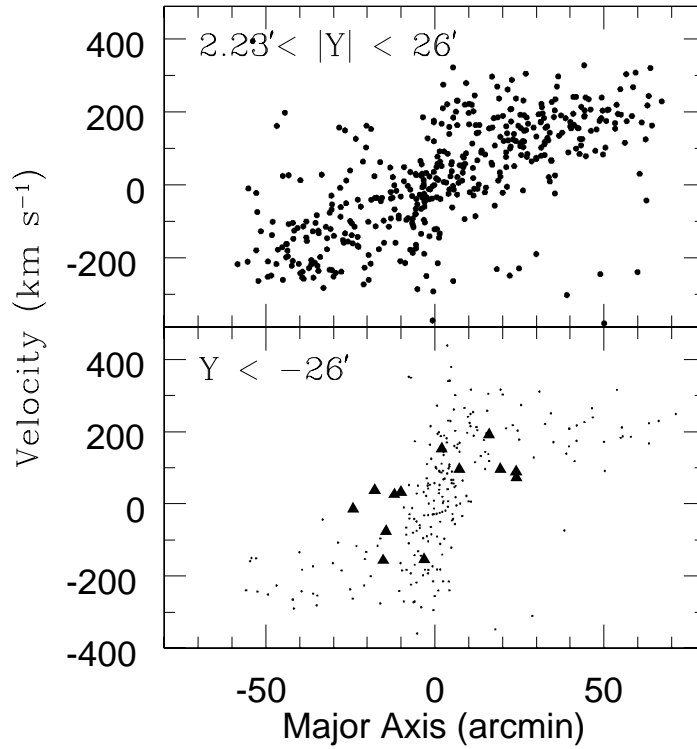
Figure 7. Line-of-sight velocity distributions for PNe with $2.23'(0.5 kpc) < |Y| < 26'$ (5.8 kpc) (upper panel) and $Y < -26'$ (lower panel). In the lower panel, the data with $Y < 26'$ are shown as triangles, and the data with $|Y| < 2.23'$ are also plotted for comparison. See text for a discussion.
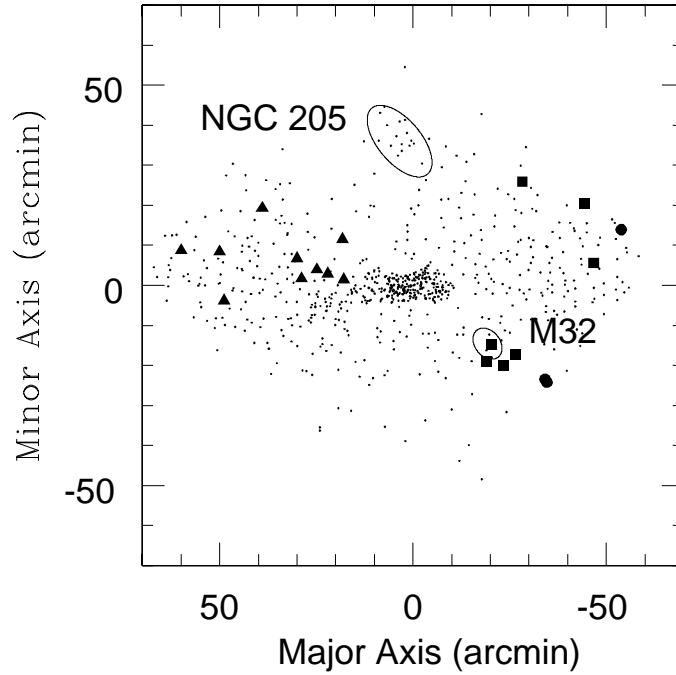
Figure 8. The spatial distribution of velocity outliers from Figure 5 compared with the distribution of our full sample (points). PNe with $X > 10'$ and $V < -150 km s^{-1}$ are shown as black triangles; those with $X < -10'$ and $V > 100 km s^{-1}$ are shown as black squares while those with $X < -10'$ and $V > 300 km s^{-1}$ are shown as black discs. The positions of M32 and NGC205 are indicated - their angular sizes and position angles are taken from de Vaucouleurs et al. (1991).

4   CONCLUSIONS

PNe velocities provide an important tool for investigating the detailed kinematics of galaxies, and we have shown that we can measure the velocities of large samples of PNe to an accuracy of 6-10 km s^{-1}. From our velocities in M31 we show that the stellar rotation curve agrees in the outer region with the published HI rotation curves, with a rotation velocity of ≈ 200 km s^{-1} at our outer limit of 50 arcmin (12 kpc). In the inner region the PNe show somewhat less rotation than the gas, in agreement with the predictions of asymmetric drift models. Figure 8 shows that the PNe velocity dispersion drops from ~ 130 km/s at the galaxy center to ~ 50 km/s at 50 arcmin (~ 11 kpc) along the major axis. As noted earlier, and in agreement with HK04, we find no evidence for a dynamically hot PNe halo with a significant velocity dispersion. This is in contrast to the M31 globular clusters, which have a global velocity dispersion of ~ 150 km/s, larger than that of the PNe (Perrett et al. 2002; unfortunately Perrett et al. do not present the radial profile for the M31 globular cluster velocity dispersion). The M31 globular clusters have a rotation velocity of ~ 140 km/s, lower than found here for the disk PNe (~ 200 km/s), though the metal-rich clusters have a higher rotation velocity of 160 ± 20 km/s. We provide confirmation of the kinematic subpopulation, counter-rotating with respect to the disk and the main bulge, found by Merrett *et al.* (2003) and identified with the extension through the plane of the southern stream of M31. Future analysis of the current dataset, combined with those of Merrett *et al.* (2006) and HK04 promise to yield a much more complete kinematic, dynamical and mass model of M31.

REFERENCES

Arnaboldi, M., Méndez, R. H., Capaccioli, M., Ciardullo, R., Ford, H. C., Gerhard, O., Hui, X., Jacoby, G. H., Kudritzki, R. P., Quinn, P. J. (1996). *ApJ*, 472, 145.

Arnaboldi, M., Freeman, K.C., Gerhard, O., Matthias, M., Kudritzki, R. P., Méndez, R.H., Capaccioli, M., Ford, H. C. (1998). *ApJ*, 507, 759.

Belokurov, V., An, J., Evans, N.W., Hewett, P., Baillon, P., Novati, S. Calchi, Carr, B.J., Créžé, M., Giraud-Héraud, Y., Gould, A., Jetzer, Ph., Kaplan, J., Kerins, E., Paulin-Henriksson, S., Smartt, S. J., Stalin, C.S., Tsapras, Y., Weston, M.J. (2005) *MNRAS*, 357, 17.

Bender, R., Kormendy, J., Bower, G., Green. R., Thomas, J., Danks, A.C., Gull, T., Hutchings, J.B., Joseph, C.L., Kaiser, M.E., Lauer, T.R., Nelson, C.H., Richstone, D., Weistrop, D., Woodgate, B. (2005). *ApJ*, 631, 280.

Braun, R. (1991). *ApJ*, 372, 54.

Carter, D., Jenkins, C.R., (1993). *MNRAS*, 263, 1049.

Ciardullo, R., Jacoby, G. H., Ford, H. C., Neill, J. D. (1989). *ApJ*, 339, 53.

Crane, P.C., Dickel, J.R., Cowan, J. (1992) *ApJ Lett*, 390, L9.

Crotts, A.P.S. (1992) *ApJ Lett*, 399, 43.

Cseresnjes, P., Crotts, A.P.S., de Jong, J.T.A., Bergier, A., Baltz, E.A., Gyuk, G., Kuijken, K., Widrow, L.M. (2005) *ApJ Lett*, 633, 105.

de Jong, J.T.A., Kuijken, K., Crotts, A.P.S., Sackett, P.D., Sutherland, W.J., Uglesich, R.R., Baltz, E.A., Cseresnjes, P., Gyuk, G., Widrow, L. M. (2004) *A&A*, 417, 461.

de Vaucouleurs, G. (1948) *Ann Ap*, 11, 247.

de Vaucouleurs, G., de Vaucouleurs, A., Corwin, H. G., Buta, R. J., Paturel, G., Fouque, P., (1991) Third Reference Catalogue of Bright Galaxies, Volume 1-3, XII, Springer-Verlag Berlin Heidelberg New York.

Douglas, N.G., Gerssen, J., Kuijken, K., Merrifield, M.R. (2000) *MNRAS*, 316, 795.

Douglas, N.G., Arnaboldi, M., Freeman, K.C., Kuijken, K., Merrifield, M. R., Romanowsky, A.J., Taylor, K., Capaccioli, M., Axelrod, T., Gilmozzi, R., Hart, J., Bloxham, G., Jones, D. (2002) *PASP*, 114, 1234.

Dressler, A., Smail, I., Poggianti, B.M., Butcher, H.R., Couch, W.J., Ellis, R.S., Oemler, A. Jr. (1999) *ApJ supp*, 122, 51.

Evans, N.W., Wilkinson, M.I. (2000). *MNRAS*, 316, 929.

Evans, N.W., Wilkinson, M.I., Guhathakurta, P., Grebel, E.K., Vogt, S.S. (2000) *ApJ* 540, 9.

Evans, N. W., Wilkinson, M. I., Perrett, K. M., Bridges, T. J. (2003) **ApJ**, 583, 752.

Federici, L., Bonoli, F., Ciotti, L., Fusi-Pecci, F., Marano, B., Lipovetsky, V. A., Niezvestny, S. I., Spassova, N. (1993) *A&A*, 274, 87.

Ferguson, A.M.N., Irwin, M.J., Ibata, R.A., Lewis, G.F., Tanvir, N.R. (2002) *AJ*, 124, 1452.

Ford, H.C., Jacoby, G.H. (1978) *ApJ suppl*, 38, 351.

Gebhardt, K., Richstone, D.O., Ajhar, E.A., Lauer, T.R., Byun, Y.-I., Kormendy, J., Dressler, A., Faber, S.M., Grillmair, C., Tremaine, S. (1996) *AJ*, 112, 105.

Gerssen, J., Kuijken, K., Merrifield, M.R. (2000) *MNRAS*, 317, 545.

Huchra, J.P., Brodie, J.P., Kent, S.M. (1991) *ApJ*, 370, 495.

Hui, X., Ford, H.C., Freeman, K.C., Dopita, M.A. (1995) *ApJ*, 449, 592.

Hurley-Keller, D., Morrison, H.L., Harding, P., Jacoby, G.H. (2004) *ApJ*, 616, 804.

Ibata, R., Irwin, M., Lewis, G., Ferguson, A. M. N., Tanvir, N. (2001) *Nature*, 412, 49.

Ibata, R., Chapman, S., Ferguson, A.M.N., Irwin, M.J.,Lewis, G.F., McConnachie, A. (2004) *MNRAS*, 351, 117.

Ibata, R., Chapman, S., Ferguson, A.M.N., Lewis, G.F., Irwin, M.J., Tanvir, N.R. (2005) *ApJ*, 634, 287.

Irwin, M.J., Ferguson, A.M.N., Ibata, R.A., Lewis, G.F., Tanvir, N.R. (2005) *ApJ Lett*, 628, L105.

Jablonka, P., Bica, E., Bonatto, C., Bridges, T. J., Langlois, M., Carter, D. (1998) *A&A*, 335, 867.

Kent. S.M. (1989). *AJ*, 97, 1614.

Kent, S.M., Huchra, J.P., Stauffer, J. (1989). *AJ*, 98, 2080.

Kerins, E., Carr, B.J., Evans, N.W., Hewett, P., Lastennet, E., Le Du, Y., Melchior, A.-L., Smartt, S.J., Valls-Gabaud, D. (2001) *MNRAS*, 323, 13.

Kerins, E., An, J., Evans, N. W., Baillon, P., Carr, B. J., Giraud-Héraud, Y., Gould, A., Hewett, P., Kaplan, J., Paulin-Henriksson, S., Smartt, S.J., Tsapras, Y., Valls-Gabaud, D. (2003) *ApJ*, 598, 993.

Kormendy, J. (1988). *ApJ*, 325, 128.

Kormendy, J., Bender, R. (1999). *ApJ*, 522, 722.

Lauer, T.R., Faber, S. M., Groth, E. J., Shaya, E. J., Campbell, B., Code, A., Currie, D. G., Baum, W. A., Ewald, S. P., Hester, J. J., Holtzman, J. A., Kristian, J., Light, R. M., Ligynds, C. R., O'Neil, E. J., Jr., Westphal, J. A. (1993) *AJ*, 106, 1436.

McElroy, D.B. (1983). *ApJ*, 270, 485.

Méndez, R.H., Riffeser, A., Kudritzki, R.-P., Matthias, M., Freeman, K.C., Arnaboldi, M., Capaccioli, M., Gerhard, O.E. (2001) *ApJ*, 563, 135.

Merrett, H.R., Kuijken, K., Merrifield, M.R., Romanowsky, A.J., Douglas, N.G., Napolitano, N.R., Arnaboldi, M., Capaccioli, M., Freeman, K.C., Gerhard, O., Evans, N. W., Wilkinson, M. I., Halliday, C., Bridges, T.J., Carter, D. (2003) *MNRAS*, 346, L62.

Merrett, H. R., et al., (2003) *MNRAS*, 346, L62.

Merrett, H.R., *et al.* (2006) *MNRAS*, submitted.

Merritt, D. (1993) *ApJ*, 413, 79.

Merritt, D. (1996) *AJ*, 112, 1085.

Merritt, D., Saha, P. (1993). *ApJ*, 409, 75.

Monet, D., Bird, A., Canzian, B., Dahn, C., Guetter, H., Harris, H., Henden, A., Levine, S., Luginbuhl, C., Monet, A. K. B., Rhodes, A., Riepe, B., Sell, S., Stone, R., Vrba, F., Walker, R. (1996). *A Catalog of Astrometric Standards*, U.S. Naval Observatory, Washington DC.

Moore, B., Calcáneo-Roldán, C., Stadel, J., Quinn, T., Lake, G., Ghigna, S., Governato, F. (2001) *Phys Rev D*, 64, 3508.

Morrison, H. L., Harding, P., Perrett, K., Hurley-Keller, D., (2004) *ApJ*, 603, 87.

Ostriker, J.P., Peebles, P.J.E., Yahil, A. (1974) *ApJ Lett*, 193, L1.

Parry, I.R., Lewis, I.J., Sharples, R.M., Dodsworth, G.N., Webster, J., Gellatly, D.W.; Jones, L.R., Watson, F.G. (1994) *Proc SPIE*, 2198, 125.

Peng, E.W., Ford, H.C., Freeman, K.C. (2004) *ApJ*, 602, 685.

Perrett, K.M., Bridges, T.J., Hanes, D.A., Irwin, M.J., Brodie, J.P., Carter, D., Huchra, J.P., Watson, F. G. (2002) *AJ*, 123, 2490.

Perrett, K.M., Stiff, D.A., Hanes, D.A., Bridges, T.J. (2003) *ApJ*, 589, 790.

Poggianti, B.M., von der Linden, A., De Lucia, G., Desai, V., Simard, L., Halliday, C., Aragon-Salamanca, A., Bower, R., Varela, J., Best, P., Clowe, D.I., Dalcanton, J., Jablonka, P., Milvang-Jensen, B., Pello, R., Rudnick, G., Saglia, R., White, S.D.M., Zaritsky D. (2006) *ApJ* in press, (astro-ph/0512391).

Pritchet, C.J., van den Bergh, S. (1994) *AJ*, 107, 1730.

Riffeser, A., Fliri, Jürgen, Bender, R., Seitz, S., Gössl, C.A. (2003) *ApJ*, 599, 17.

Roberts, M.S., Whitehurst, R.N. (1975) *ApJ*, 201, 327.

Rubin, V.C., Ford, W.K. Jr. (1970) *ApJ*, 159, 379.

van der Marel, R.P., Rix, H.-W., Carter, D., Franx, M., White, S.D.M., de Zeeuw, T. (1994) *MNRAS*, 268, 521.

Widrow, L.M., Dubinski, J. (2005) *ApJ*, 631, 838.

Worswick, S.P., Gellatly, D.W., Ferneyhough, N.K., King, D.L., Weise, A.J., Bingham, R.G., Oates, A.P. (1995) *Proc SPIE*, 2476, 46.

APPENDIX A: PLANETARY NEBULAE VELOCITY MEASUREMENTS

Table A1: Positions and Velocities of Planetary Nebulae.

Identifier	RA (J2000)	Dec (J2000)	cz (km/s)	error (km/s)	Major axis Arcmin	Minor Axis Arcmin	Radius Arcmin	Azimuth Degrees	N Obs
PN_8_1_1	00 38 43.65	41 14 11.2	-271.0	8.2	-27.34	36.09	45.28	127.14	1
PN_8_4_1	00 38 46.17	41 28 19.4	-243.4	6.0	-15.40	43.67	46.31	109.42	1
PN_12_4_1	00 38 48.37	40 45 31.7	-437.0	6.0	-50.50	19.19	54.02	159.20	1
PN_12_4_2	00 38 49.51	40 44 25.4	-573.2	11.6	-51.29	18.38	54.48	160.28	1
PN_12_1_1	00 38 51.09	40 42 3.8	84.6	13.5	-53.07	16.80	55.66	162.43	1
PN_12_4_5	00 38 54.40	40 53 38.5	-111.8	8.2	-43.16	22.82	48.82	152.13	1
PN_7_1_2	00 39 1.10	41 51 11.5	-219.8	8.2	5.05	54.28	54.51	84.68	1
PN_12_1_2	00 39 4.49	40 34 29.7	-527.2	8.2	-57.88	10.43	58.81	169.78	1
PN_12_1_6	00 39 5.31	40 41 45.8	-384.0	6.0	-51.79	14.41	53.76	164.45	1
PN_12_1_5	00 39 6.23	40 38 19.3	-319.6	11.6	-54.53	12.32	55.91	167.27	1
PN_8_1_3	00 39 7.98	41 12 25.4	-239.9	8.2	-26.21	31.32	40.84	129.93	1
PN_12_1_4	00 39 10.09	40 37 27.8	-520.4	6.0	-54.83	11.23	55.97	168.42	1
PN_12_3_2	00 39 11.11	40 56 58.2	-297.0	8.2	-38.63	22.10	44.50	150.23	1
PN_12_4_6	00 39 13.05	40 50 7.2	-285.2	9.9	-44.07	17.92	47.58	157.87	1
PN_12_4_7	00 39 17.13	40 45 13.7	-558.6	6.0	-47.67	14.52	49.83	163.06	1
PN_8_1_5	00 39 22.62	41 6 57.2	-377.5	6.0	-29.17	25.95	39.04	138.34	1
PN_12_4_13	00 39 22.73	40 48 44.1	-570.4	6.0	-44.18	15.63	46.86	160.52	1
PN_8_1_4	00 39 23.47	41 9 38.7	-152.4	6.0	-26.86	27.34	38.33	134.48	1
PN_12_3_5	00 39 24.54	41 4 32.5	-425.0	6.0	-30.95	24.29	39.34	141.87	1
PN_12_1_7	00 39 25.43	40 38 25.0	-489.3	8.2	-52.40	9.37	53.23	169.86	1
PN_12_4_8	00 39 26.17	40 44 26.7	-411.2	6.0	-47.35	12.67	49.01	165.02	1
PN_12_4_14	00 39 26.55	40 53 37.7	-428.0	11.6	-39.73	17.80	43.54	155.86	1
PN_12_4_11	00 39 29.10	40 52 2.0	-435.3	6.0	-40.78	16.50	43.99	157.96	1
PN_12_4_10	00 39 31.20	40 51 25.4	-457.5	6.0	-41.05	15.83	44.00	158.91	1
PN_12_4_15	00 39 34.55	40 49 11.8	-417.0	6.0	-42.53	14.05	44.79	161.72	1
PN_8_4_2	00 39 34.90	41 23 44.2	-253.4	6.0	-14.02	33.55	36.36	112.68	1
PN_12_3_4	00 39 35.18	40 55 53.8	-463.8	6.0	-36.94	17.74	40.98	154.34	1
PN_12_4_17	00 39 40.37	40 47 27.1	-471.5	6.0	-43.35	12.15	45.02	164.34	1
PN_12_3_7	00 39 42.54	41 2 21.0	-455.7	6.0	-30.84	20.25	36.89	146.70	1
PN_12_3_8	00 39 43.53	41 3 30.6	-430.7	6.0	-29.77	20.76	36.30	145.12	1
PN_12_1_9	00 39 43.97	40 35 41.4	-460.7	8.2	-52.65	4.93	52.88	174.65	1
PN_12_1_10	00 39 44.84	40 33 51.1	-460.4	9.9	-54.07	3.75	54.20	176.03	1
PN_12_1_8	00 39 45.40	40 31 42.2	-549.5	8.2	-55.78	2.45	55.84	177.49	1
PN_8_1_7	00 39 48.20	41 8 42.1	-297.6	6.0	-25.00	22.97	33.95	137.42	1
PN_8_1_8	00 39 48.57	41 10 40.8	-447.7	6.0	-23.33	24.04	33.50	134.14	1
PN_2_2_17	00 39 49.07	40 42 39.6	-148.1	8.2	-46.36	8.08	47.06	170.11	1
PN_8_4_3	00 39 49.26	41 24 9.5	-258.5	6.0	-12.15	31.57	33.82	111.05	1
PN_12_1_13	00 39 50.16	40 40 40.6	-447.1	6.0	-47.88	6.79	48.36	171.93	1
PN_8_3_2	00 39 50.70	41 30 43.0	-263.8	6.0	-6.59	35.06	35.68	100.65	1
PN_12_3_9	00 39 50.78	40 55 49.3	-437.3	6.0	-35.33	15.27	38.49	156.62	1
PN_2_2_48	00 39 50.82	40 53 23.4	-453.9	13.5	-37.33	13.89	39.83	159.59	1
PN_8_4_6	00 39 51.25	41 27 7.1	-480.9	6.0	-9.50	32.94	34.28	106.09	1
PN_8_1_6	00 39 51.38	41 13 38.3	-369.4	6.0	-20.59	25.28	32.60	129.17	1
PN_12_1_16	00 39 53.97	40 31 56.5	-469.3	8.2	-54.66	1.24	54.68	178.70	1
PN_12_4_21	00 39 55.06	40 45 52.0	-505.7	6.0	-43.08	8.96	44.00	168.25	1
PN_8_3_3	00 39 56.60	41 35 19.0	-227.6	6.0	-2.18	36.76	36.82	93.39	1
PN_7_1_3	00 39 56.90	41 43 6.7	-315.4	6.0	4.28	41.13	41.35	84.07	1
PN_12_3_13	00 39 56.98	41 5 7.7	-317.8	6.0	-27.00	19.59	33.36	144.05	1
PN_12_1_15	00 39 58.26	40 34 5.0	-553.3	8.2	-52.44	1.78	52.47	178.05	1
PN_8_1_9	00 39 58.85	41 6 42.3	-442.8	6.0	-25.51	20.19	32.53	141.64	1
PN_7_1_6	00 40 0.55	41 49 19.3	-212.0	6.0	9.78	44.09	45.16	77.50	1
PN_12_4_20	00 40 0.83	40 44 55.5	-490.2	6.0	-43.23	7.53	43.88	170.12	1
PN_12_1_11	00 40 1.86	40 37 28.2	-561.3	6.0	-49.26	3.14	49.36	176.35	1
PN_12_4_25	00 40 3.09	40 50 36.5	-567.3	8.2	-38.31	10.40	39.70	164.81	1
PN_7_1_4	00 40 3.40	41 43 59.9	-194.3	6.0	5.69	40.64	41.03	82.02	1
PN_2_2_21	00 40 5.18	40 42 16.0	-481.0	6.0	-44.95	5.34	45.27	173.22	1

Table A1: Positions and Velocities of Planetary Nebulae.

PN_12_1_17	00 40 8.03	40 32 11.9	-331.9	6.0	-52.94	-0.82	52.94	180.88	1
PN_7_1_5	00 40 8.88	41 40 43.8	-240.5	6.0	3.58	37.94	38.11	84.61	1
PN_7_1_7	00 40 10.48	41 49 18.8	-177.3	6.0	10.82	42.56	43.92	75.74	1
PN_8_4_9	00 40 10.60	41 21 23.7	-220.7	6.0	-12.16	26.70	29.34	114.48	1
PN_12_3_19	00 40 10.82	40 54 38.6	-531.5	6.0	-34.16	11.49	36.04	161.41	1
PN_12_3_20	00 40 11.29	40 54 55.0	-435.3	6.0	-33.88	11.57	35.80	161.15	1
PN_8_3_9	00 40 13.57	41 38 41.9	-229.2	6.0	2.41	36.07	36.15	86.18	1
PN_12_1_21	00 40 13.73	40 35 41.7	-562.0	6.0	-49.44	0.28	49.44	179.68	1
PN_12_1_22	00 40 14.54	40 38 50.3	-535.8	6.0	-46.77	1.94	46.81	177.63	1
PN_8_3_10	00 40 14.56	41 37 42.1	-230.6	6.0	1.69	35.35	35.39	87.26	1
PN_12_3_17	00 40 15.60	40 58 29.7	-542.7	6.0	-30.47	12.93	33.10	157.01	1
PN_8_4_7	00 40 15.82	41 28 22.8	-317.4	6.0	-5.85	29.86	30.43	101.08	1
PN_1_2_9	00 40 16.68	41 17 30.3	-354.6	8.2	-14.71	23.56	27.77	121.98	1
PN_12_3_14	00 40 16.73	41 4 28.7	-360.2	6.0	-25.43	16.15	30.12	147.58	1
PN_12_3_16	00 40 17.22	40 59 45.8	-561.2	6.0	-29.26	13.40	32.18	155.39	1
PN_7_1_9	00 40 17.50	41 45 59.0	-217.1	6.0	8.82	39.60	40.57	77.44	1
PN_12_4_38	00 40 18.46	40 52 0.9	-564.3	6.0	-35.50	8.81	36.58	166.07	1
PN_8_3_6	00 40 20.35	41 38 17.4	-227.2	6.0	2.79	34.79	34.90	85.42	1
PN_7_1_10	00 40 21.54	41 42 26.2	-282.6	6.0	6.33	36.96	37.50	80.28	1
PN_8_1_12	00 40 21.81	41 10 4.5	-246.0	6.0	-20.28	18.54	27.48	137.56	1
PN_12_4_34	00 40 22.11	40 48 49.8	-410.2	6.0	-37.73	6.43	38.27	170.33	1
PN_12_4_30	00 40 23.50	40 44 0.6	-600.4	6.0	-41.55	3.47	41.69	175.22	1
PN_12_3_21	00 40 24.70	40 58 2.9	-363.3	6.0	-29.87	11.26	31.92	159.34	1
PN_12_4_31	00 40 24.94	40 47 17.6	-423.7	6.0	-38.69	5.12	39.03	172.47	1
PN_7_1_11	00 40 25.53	41 40 6.8	-227.5	6.0	4.84	35.03	35.36	82.13	1
PN_12_4_36	00 40 25.74	40 51 45.4	-414.0	6.0	-34.93	7.53	35.73	167.84	1
PN_12_1_24	00 40 25.74	40 37 6.1	-526.8	6.0	-46.99	-0.80	47.00	180.98	1
PN_12_3_23	00 40 25.81	41 1 9.1	-370.7	6.0	-27.19	12.85	30.08	154.70	1
PN_8_4_10	00 40 26.25	41 20 27.6	-344.8	6.0	-11.26	23.75	26.29	115.36	1
PN_8_3_12	00 40 28.81	41 33 0.6	-320.9	6.0	-0.66	30.49	30.50	91.23	1
PN_12_3_24	00 40 30.08	41 1 20.2	-460.9	6.0	-26.58	12.30	29.29	155.18	1
PN_12_1_23	00 40 30.81	40 36 53.9	-487.2	6.0	-46.61	-1.71	46.64	182.10	1
PN_2_2_29	00 40 30.82	40 42 30.1	-574.9	6.0	-42.00	1.48	42.03	177.99	1
PN_12_4_33	00 40 30.89	40 45 46.9	-552.1	6.0	-39.30	3.33	39.44	175.16	1
PN_8_3_16	00 40 32.24	41 39 2.8	-241.8	6.0	4.67	33.39	33.72	82.03	1
PN_12_3_26	00 40 33.28	40 55 58.6	-386.4	6.0	-30.65	8.75	31.88	164.06	1
PN_12_1_29	00 40 33.75	40 32 46.0	-519.8	6.0	-49.69	-4.52	49.90	185.19	1
PN_8_1_16	00 40 33.87	41 8 34.8	-582.7	6.0	-20.22	15.83	25.68	141.95	1
PN_12_4_40	00 40 35.18	40 50 7.3	-523.6	4.2	-35.26	5.13	35.63	171.73	2
PN_12_4_41	00 40 35.48	40 45 16.8	-492.5	6.0	-39.21	2.33	39.28	176.60	1
PN_11_1_2	00 40 36.33	41 42 2.5	-254.8	6.0	7.57	34.47	35.29	77.61	1
PN_1_1_1	00 40 39.02	41 14 38.9	-345.2	13.5	-14.68	18.48	23.60	128.46	1
PN_2_4_9	00 40 39.91	40 43 37.1	-444.0	6.0	-40.10	0.69	40.11	179.01	1
PN_1_3_1	00 40 40.63	41 39 5.7	-233.3	6.0	5.61	32.13	32.62	80.10	1
PN_11_1_3	00 40 41.29	41 45 17.1	-233.1	8.2	10.77	35.55	37.14	73.15	1
PN_2_3_6	00 40 41.52	40 55 34.6	-543.3	6.0	-30.10	7.24	30.95	166.47	1
PN_1_3_3	00 40 42.67	41 29 38.7	-265.8	8.2	-1.95	26.44	26.52	94.22	1
PN_2_4_4	00 40 43.41	40 52 8.1	-592.3	6.0	-32.72	4.99	33.10	171.32	1
PN_1_4_2	00 40 43.74	41 18 40.4	-376.7	6.0	-10.86	20.04	22.79	118.46	1
PN_1_4_3	00 40 43.93	41 22 10.9	-299.6	6.0	-7.95	22.00	23.40	109.88	1
PN_2_3_10	00 40 44.36	40 59 37.0	-468.2	6.0	-26.47	9.10	27.99	161.02	1
PN_2_1_3	00 40 44.38	40 40 30.8	-518.4	6.0	-42.18	-1.77	42.21	182.40	1
PN_2_4_6	00 40 45.66	40 49 13.5	-591.4	6.0	-34.87	2.99	35.00	175.10	1
PN_2_4_11	00 40 46.18	40 47 50.1	-558.9	6.0	-35.96	2.12	36.02	176.63	1
PN_2_3_5	00 40 48.08	41 2 2.0	-415.2	6.0	-24.08	9.90	26.04	157.65	1
PN_2_4_12	00 40 48.42	40 43 33.2	-548.0	6.0	-39.24	-0.67	39.25	180.98	1
PN_1_1_3	00 40 49.11	41 10 48.4	-423.4	6.0	-16.76	14.73	22.31	138.68	1
PN_2_1_5	00 40 49.56	40 39 46.5	-414.0	6.0	-42.22	-3.00	42.33	184.06	1
PN_1_4_1	00 40 50.45	41 23 35.0	-322.3	6.0	-6.11	21.80	22.64	105.65	1
PN_2_3_7	00 40 50.63	40 54 56.8	-449.6	6.0	-29.63	5.47	30.13	169.54	1

Table A1: Positions and Velocities of Planetary Nebulae.

PN_1_1_2	00 40 53.30	41 16 37.9	-288.4	6.0	-11.52	17.40	20.87	123.50	1
PN_2_4_8	00 40 54.01	40 46 39.9	-483.4	6.0	-36.08	0.23	36.08	179.63	1
PN_2_4_2	00 40 54.38	40 48 10.6	-564.0	6.0	-34.80	1.03	34.81	178.30	1
PN_11_1_1	00 40 54.66	41 48 15.8	-357.3	6.0	14.63	35.20	38.12	67.42	1
PN_2_3_4	00 40 55.91	41 3 8.5	-350.3	6.0	-22.33	9.32	24.19	157.35	1
PN_2_1_9	00 40 57.24	40 36 7.4	-508.1	6.0	-44.40	-6.27	44.84	188.04	1
PN_2_3_2	00 40 57.41	41 1 2.8	-470.1	6.0	-23.89	7.89	25.16	161.72	1
PN_2_3_3	00 40 57.58	41 0 1.8	-270.6	6.0	-24.71	7.29	25.76	163.57	1
PN_1_1_6	00 40 58.49	41 9 6.9	-346.1	6.0	-17.14	12.32	21.11	144.30	1
PN_1_3_4	00 40 58.75	41 29 32.5	-286.7	6.0	-0.32	23.91	23.91	90.77	1
PN_1_1_7	00 41 3.09	41 11 57.8	-468.5	6.0	-14.31	13.23	19.49	137.24	1
PN_2_3_13	00 41 3.40	40 55 53.6	-547.8	6.0	-27.48	4.03	27.78	171.66	1
PN_2_1_11	00 41 3.73	40 41 13.5	-564.0	6.0	-39.50	-4.38	39.74	186.33	1
PN_2_4_13	00 41 3.79	40 48 50.4	-353.3	6.0	-33.24	-0.05	33.24	180.09	1
PN_2_4_15	00 41 5.73	40 48 11.1	-281.8	6.0	-33.57	-0.73	33.57	181.24	1
PN_2_3_20	00 41 9.20	41 3 43.3	-536.8	4.2	-20.43	7.59	21.79	159.62	2
PN_1_4_4	00 41 9.82	41 20 45.6	-274.5	6.0	-6.36	17.20	18.34	110.29	1
PN_2_4_19	00 41 10.18	40 51 44.1	-473.8	6.0	-30.17	0.60	30.18	178.85	1
PN_2_1_18	00 41 11.62	40 34 14.5	-472.2	11.6	-44.39	-9.59	45.41	192.19	1
PN_2_4_18	00 41 11.85	40 43 24.8	-516.0	6.0	-36.83	-4.40	37.09	186.81	1
PN_2_1_17	00 41 12.39	40 35 58.0	-531.5	6.0	-42.89	-8.73	43.77	191.50	1
PN_2_1_13	00 41 13.50	40 42 15.6	-537.9	6.0	-37.60	-5.31	37.97	188.04	1
PN_2_4_16	00 41 13.66	40 45 47.9	-545.7	6.0	-34.67	-3.32	34.83	185.47	1
PN_1_1_21	00 41 15.07	41 7 26.8	-345.0	6.0	-16.73	8.80	18.91	152.26	1
PN_1_4_6	00 41 15.72	41 27 19.8	-321.9	6.0	-0.33	20.04	20.04	90.94	1
PN_1_1_16	00 41 16.91	41 12 11.6	-262.2	6.0	-12.64	11.22	16.90	138.39	1
PN_1_4_9	00 41 17.65	41 18 45.4	-400.9	8.2	-7.17	14.85	16.49	115.76	1
PN_2_1_16	00 41 18.69	40 37 42.6	-526.3	6.0	-40.77	-8.71	41.69	192.06	1
PN_2_4_26	00 41 19.08	40 53 41.8	-494.7	6.0	-27.60	0.34	27.60	179.29	1
PN_2_4_27	00 41 19.34	40 52 20.5	-417.5	6.0	-28.68	-0.47	28.69	180.94	1
PN_11_1_5	00 41 19.78	41 41 9.8	-358.4	6.0	11.47	27.30	29.61	67.21	1
PN_2_4_32	00 41 19.91	40 44 57.9	-442.6	6.0	-34.68	-4.77	35.01	187.83	1
PN_2_3_32	00 41 23.13	41 4 12.5	-350.5	8.2	-18.53	5.71	19.39	162.88	1
PN_2_4_23	00 41 23.32	40 50 51.9	-551.1	6.0	-29.47	-1.93	29.53	183.75	1
PN_1_1_11	00 41 23.43	41 14 28.0	-402.2	6.0	-10.07	11.51	15.30	131.18	1
PN_2_3_38	00 41 25.26	40 56 2.2	-547.4	6.0	-25.01	0.72	25.02	178.36	1
PN_1_4_7	00 41 25.39	41 28 22.2	-293.5	6.0	1.56	19.14	19.20	85.34	1
PN_2_1_15	00 41 26.47	40 32 45.0	-283.3	8.2	-44.00	-12.76	45.82	196.17	1
PN_2_4_31	00 41 26.87	40 43 15.8	-392.9	6.0	-35.33	-6.82	35.98	190.93	1
PN_2_3_35	00 41 27.01	40 58 6.3	-426.9	6.0	-23.12	1.62	23.18	175.98	1
PN_2_3_29	00 41 28.19	41 2 30.3	-570.1	8.2	-19.38	3.95	19.78	168.47	1
PN_1_4_8	00 41 28.81	41 26 47.7	-274.3	6.0	0.63	17.72	17.73	87.96	1
PN_1_1_22	00 41 29.41	41 6 38.5	-247.4	8.2	-15.86	6.12	17.00	158.88	1
PN_1_1_23	00 41 31.09	41 9 36.0	-424.4	6.0	-13.25	7.55	15.25	150.31	1
PN_2_3_24	00 41 31.17	41 1 11.0	-443.1	6.0	-20.15	2.74	20.33	172.26	1
PN_2_3_25	00 41 32.24	41 0 11.9	-536.5	6.0	-20.84	2.01	20.94	174.49	1
PN_2_3_39	00 41 33.19	40 55 48.5	-572.9	6.0	-24.34	-0.64	24.35	181.52	1
PN_1_1_25	00 41 33.71	41 12 56.3	-394.0	6.0	-10.22	9.05	13.66	138.47	1
PN_2_4_30	00 41 35.26	40 45 49.2	-486.6	6.0	-32.32	-6.67	33.00	191.65	1
PN_2_3_34	00 41 39.07	41 4 45.0	-486.2	9.9	-16.37	3.55	16.75	167.76	1
PN_2_4_34	00 41 39.96	40 46 47.7	-339.3	6.0	-31.01	-6.84	31.76	192.44	1
PN_2_4_38	00 41 41.18	40 52 46.7	-465.2	6.0	-25.97	-3.61	26.22	187.92	1
PN_1_1_27	00 41 42.94	41 16 36.7	-340.1	6.0	-6.22	9.73	11.54	122.58	1
PN_2_3_47	00 41 43.90	41 4 36.1	-405.8	11.6	-15.97	2.72	16.20	170.34	1
PN_1_4_13	00 41 45.38	41 20 36.5	-313.2	6.0	-2.67	11.63	11.94	102.95	1
PN_2_3_45	00 41 45.45	40 58 36.2	-463.0	6.0	-20.73	-0.95	20.75	182.62	1
PN_1_4_16	00 41 45.89	41 26 34.4	-443.1	6.0	2.28	14.96	15.13	81.35	1
PN_2_3_48	00 41 46.06	41 3 11.9	-426.2	6.0	-16.89	1.58	16.96	174.65	1
PN_2_3_41	00 41 46.25	41 0 34.4	-510.5	6.0	-19.02	0.05	19.02	179.84	1
PN_11_1_6	00 41 48.35	41 43 30.2	-316.9	9.9	16.43	24.26	29.30	55.88	1

Table A1: Positions and Velocities of Planetary Nebulae.

PN_2_4_36	00 41 48.92	40 48 53.5	-397.2	6.0	-28.32	-7.04	29.18	193.95	1
PN_1_1_28	00 41 49.66	41 11 21.6	-341.5	6.0	-9.80	5.69	11.34	149.88	1
PN_1_1_45	00 41 50.14	41 7 34.0	-401.6	6.0	-12.87	3.45	13.32	165.00	1
PN_2_1_23	00 41 51.79	40 37 32.8	-527.7	6.0	-37.32	-13.96	39.85	200.51	1
PN_1_4_17	00 41 52.35	41 25 32.2	-218.0	6.0	2.12	13.38	13.54	81.01	1
PN_1_3_8	00 41 54.55	41 36 16.5	-143.5	6.0	11.16	19.18	22.19	59.79	1
PN_2_1_22	00 41 54.96	40 40 22.4	-507.6	6.0	-34.66	-12.84	36.96	200.33	1
PN_1_3_7	00 41 56.79	41 37 5.3	-196.2	13.5	12.07	19.30	22.76	57.97	1
PN_2_3_59	00 42 0.55	41 2 5.9	-585.5	6.0	-16.23	-1.29	16.28	184.54	1
PN_1_4_19	00 42 1.48	41 24 21.0	-246.1	6.0	2.12	11.29	11.49	79.36	1
PN_2_4_44	00 42 1.87	40 53 22.4	-476.4	6.0	-23.25	-6.48	24.13	195.58	1
PN_2_1_25	00 42 3.33	40 31 39.5	-551.8	11.6	-40.90	-19.13	45.15	205.07	1
PN_1_1_54	00 42 5.24	41 16 9.7	-336.4	6.0	-4.19	6.03	7.34	124.79	1
PN_1_1_71	00 42 6.63	41 11 33.0	-312.8	8.2	-7.82	3.18	8.44	157.89	1
PN_1_1_65	00 42 7.70	41 13 28.2	-425.5	8.2	-6.13	4.11	7.38	146.16	1
PN_3_2_37	00 42 9.64	40 52 35.4	-479.7	6.0	-23.05	-8.14	24.44	199.44	1
PN_1_3_13	00 42 9.91	41 35 39.4	-339.0	13.5	12.30	16.47	20.55	53.24	1
P375	00 42 10.27	41 12 38.0	-414.2	6.4	-6.54	3.24	7.30	153.68	1
P374	00 42 10.28	41 8 51.1	-494.5	4.6	-9.64	1.07	9.70	173.66	1
PN_6_2_109	00 42 10.35	41 20 45.3	-190.1	13.5	0.13	7.87	7.87	89.09	1
P296	00 42 10.48	41 16 5.6	-285.2	4.6	-3.68	5.18	6.36	125.39	1
P377	00 42 11.05	41 8 4.4	-474.3	6.4	-10.20	0.51	10.21	177.15	1
P295	00 42 11.55	41 16 11.5	-316.3	4.6	-3.49	5.08	6.16	124.50	1
PN_3_2_28	00 42 11.89	40 49 7.8	-409.0	8.2	-25.64	-10.46	27.70	202.20	1
PN_1_1_80	00 42 12.24	41 7 26.9	-551.5	8.2	-10.58	-0.03	10.58	180.19	1
PN_1_4_23	00 42 12.56	41 26 17.2	-322.1	8.2	4.90	10.70	11.77	65.39	1
P378	00 42 12.57	41 13 25.6	-390.5	3.3	-5.65	3.34	6.56	149.42	2
PN_11_3_2	00 42 12.61	42 3 42.2	-263.0	11.6	35.59	32.10	47.93	42.05	1
P379	00 42 13.15	41 9 54.2	-395.5	6.4	-8.47	1.23	8.56	171.74	1
PN_3_2_29	00 42 13.61	40 50 28.5	-424.5	6.0	-24.35	-9.96	26.31	202.25	1
P380	00 42 13.85	41 13 36.7	-283.0	4.6	-5.36	3.24	6.26	148.79	1
P381	00 42 13.86	41 8 57.9	-319.6	4.6	-9.17	0.58	9.18	176.36	1
P292	00 42 15.05	41 15 57.3	-124.1	4.6	-3.31	4.40	5.50	126.91	1
PN_1_3_14	00 42 15.14	41 39 9.6	-330.2	9.9	15.73	17.67	23.66	48.32	1
PN_2_3_64	00 42 15.15	40 55 32.0	-502.2	6.0	-20.04	-7.30	21.33	200.03	1
P382	00 42 15.72	41 12 43.4	-452.2	4.6	-5.88	2.45	6.37	157.41	1
P293	00 42 15.92	41 16 17.3	-334.2	4.6	-2.94	4.46	5.34	123.39	1
P385	00 42 16.54	41 11 7.0	-502.8	4.6	-7.11	1.40	7.25	168.85	1
PN_1_4_26	00 42 17.19	41 22 36.6	-258.1	13.5	2.38	7.88	8.23	73.19	1
PN_1_4_29	00 42 17.56	41 20 32.0	-291.9	8.2	0.72	6.64	6.67	83.82	1
P387	00 42 18.64	41 14 56.7	-253.5	4.6	-3.75	3.27	4.97	138.89	1
P291	00 42 18.65	41 16 0.9	-369.4	4.6	-2.87	3.88	4.83	126.47	1
PN_2_3_66	00 42 19.12	40 57 8.6	-285.8	5.5	-18.29	-7.00	19.58	200.94	2
P388	00 42 19.24	41 10 6.6	-257.7	4.6	-7.65	0.41	7.66	176.94	1
P389	00 42 20.09	41 15 34.3	-405.8	8.2	-3.08	3.41	4.59	132.11	1
P390	00 42 20.38	41 7 58.3	-580.7	4.6	-9.28	-0.99	9.33	186.10	1
P391	00 42 20.42	41 12 41.4	-528.0	4.6	-5.40	1.70	5.67	162.50	1
P91	00 42 20.79	41 16 53.1	-181.9	4.6	-1.93	4.05	4.48	115.43	1
P393	00 42 21.16	41 9 42.7	42.0	4.6	-7.77	-0.12	7.77	180.85	1
PN_1_4_24	00 42 21.55	41 25 19.5	-286.2	13.5	5.08	8.77	10.13	59.93	1
P395	00 42 21.68	41 9 54.5	-338.6	4.6	-7.55	-0.08	7.55	180.63	1
P97	00 42 21.83	41 14 11.1	-453.6	4.6	-4.03	2.34	4.66	149.81	1
P396	00 42 22.07	41 11 25.8	-582.0	4.6	-6.26	0.73	6.30	173.37	1
P92	00 42 22.36	41 16 4.2	-276.6	4.4	-2.42	3.34	4.13	125.97	2
P398	00 42 22.56	41 8 32.0	-375.7	4.6	-8.58	-1.01	8.64	186.69	1
P182	00 42 22.81	41 15 31.9	-412.9	4.6	-2.82	2.96	4.09	133.56	1
PN_11_1_7	00 42 22.85	41 46 0.3	-220.5	11.6	22.17	20.41	30.13	42.64	1
P400	00 42 23.18	41 13 37.3	-377.0	4.4	-4.34	1.81	4.71	157.35	2
P401	00 42 23.66	41 9 23.2	-419.0	4.6	-7.76	-0.69	7.79	185.06	1
P402	00 42 23.84	41 8 29.8	-492.9	4.6	-8.47	-1.23	8.56	188.23	1

Table A1: Positions and Velocities of Planetary Nebulae.

P149	00 42 24.39	41 12 11.4	-384.5	3.2	-5.39	0.81	5.45	171.49	3
P183	00 42 24.47	41 14 38.7	-404.6	4.6	-3.37	2.20	4.02	146.83	1
PN_1_1_88	00 42 24.63	41 7 28.2	-261.0	8.2	-9.23	-1.93	9.43	191.84	1
P404	00 42 24.65	41 10 48.4	-389.9	4.6	-6.49	-0.03	6.49	180.24	1
P148	00 42 25.01	41 12 16.3	-669.7	4.6	-5.25	0.76	5.31	171.80	1
P407	00 42 25.45	41 12 0.5	-358.9	4.6	-5.42	0.54	5.45	174.33	1
P93	00 42 25.60	41 15 42.5	-559.7	4.4	-2.37	2.63	3.55	132.00	2
P409	00 42 25.91	41 11 5.9	-351.4	4.6	-6.12	-0.05	6.12	180.51	1
P147	00 42 25.93	41 12 31.2	-441.2	4.6	-4.95	0.76	5.01	171.30	1
P410	00 42 27.00	41 9 44.4	-533.9	4.3	-7.11	-1.00	7.18	188.01	2
PN_2_4_54	00 42 27.00	40 49 40.5	-452.2	8.2	-23.56	-12.50	26.67	207.94	1
P101	00 42 27.14	41 14 54.4	-492.6	4.6	-2.86	1.94	3.46	145.91	1
P49	00 42 27.18	41 14 34.2	-341.7	4.6	-3.14	1.74	3.59	150.99	1
P47	00 42 27.76	41 16 19.2	-321.4	4.6	-1.64	2.65	3.12	121.71	1
P46	00 42 27.77	41 16 30.7	-450.4	4.6	-1.48	2.76	3.13	118.20	1
P412	00 42 28.22	41 17 35.7	-313.5	6.4	-0.54	3.31	3.36	99.33	1
P413	00 42 28.31	41 9 56.0	-321.5	4.6	-6.81	-1.09	6.90	189.10	1
P95	00 42 28.33	41 15 28.9	-399.6	4.6	-2.26	2.08	3.08	137.38	1
P414	00 42 28.46	41 9 34.3	39.9	4.6	-7.09	-1.32	7.22	190.56	1
P416	00 42 28.77	41 8 49.5	-350.6	6.4	-7.67	-1.80	7.88	193.19	1
PN_2_4_53	00 42 28.93	40 44 38.6	-160.3	8.2	-27.47	-15.68	31.63	209.71	1
PN_6_2_29	00 42 28.94	41 7 12.7	-523.9	11.6	-8.98	-2.75	9.39	197.02	1
P419	00 42 28.96	41 11 37.0	-281.3	4.6	-5.36	-0.23	5.37	182.43	1
P48	00 42 29.06	41 15 16.1	-238.8	4.3	-2.36	1.85	3.00	141.92	2
P150	00 42 29.47	41 10 49.6	-136.3	4.6	-5.96	-0.76	6.00	187.26	1
P50	00 42 29.54	41 14 4.2	-277.4	4.6	-3.29	1.09	3.47	161.69	1
P98	00 42 29.67	41 13 51.8	-507.7	4.6	-3.45	0.95	3.57	164.58	1
PN_2_3_68	00 42 29.75	41 3 30.2	-468.6	6.0	-11.93	-5.00	12.93	202.74	1
PN_2_1_33	00 42 30.58	40 34 46.5	256.0	9.9	-35.38	-21.59	41.45	211.39	1
P421	00 42 30.73	41 17 52.9	-310.0	6.4	-0.04	3.09	3.09	90.72	1
P43	00 42 31.00	41 16 24.9	-94.6	4.6	-1.21	2.21	2.52	118.77	1
PN_3_2_38	00 42 31.05	40 53 4.4	-411.0	6.3	-20.34	-11.18	23.20	208.79	2
P422	00 42 31.32	41 10 29.0	-478.8	4.6	-6.04	-1.24	6.16	191.61	1
P424	00 42 31.98	41 17 31.9	-137.7	6.4	-0.19	2.70	2.70	94.05	1
PN_3_2_5	00 42 32.18	40 33 58.3	226.8	6.0	-35.87	-22.30	42.23	211.87	1
P45	00 42 32.51	41 15 58.3	-257.0	4.6	-1.41	1.72	2.23	129.38	1
P151	00 42 32.57	41 10 14.3	-580.7	4.6	-6.10	-1.57	6.30	194.46	1
P42	00 42 32.76	41 16 32.4	-394.1	4.6	-0.92	2.01	2.21	114.61	1
P41	00 42 33.21	41 16 49.1	-482.7	4.6	-0.64	2.10	2.19	107.05	1
P51	00 42 34.12	41 15 4.4	-341.0	4.6	-1.98	0.96	2.20	154.12	1
P429	00 42 34.49	41 9 14.8	-496.0	4.6	-6.71	-2.44	7.14	199.97	1
PN_1_1_95	00 42 34.54	41 9 15.8	-489.2	13.5	-6.69	-2.44	7.12	200.01	1
P430	00 42 34.96	41 8 15.4	-487.4	4.6	-7.47	-3.08	8.08	202.40	1
P53	00 42 35.26	41 14 45.9	-259.2	4.6	-2.11	0.61	2.19	163.94	1
P432	00 42 35.73	41 18 23.0	-232.1	6.4	0.91	2.61	2.76	70.76	1
P152	00 42 35.77	41 11 1.0	-259.7	4.6	-5.12	-1.62	5.37	197.57	1
P39	00 42 36.41	41 16 56.9	-322.8	4.6	-0.19	1.68	1.69	96.53	1
P69	00 42 36.92	41 12 9.4	-597.1	4.6	-4.06	-1.15	4.22	195.74	1
P54	00 42 37.08	41 14 35.1	-503.0	4.6	-2.06	0.22	2.07	173.83	1
P37	00 42 37.19	41 16 26.3	-339.5	6.4	-0.53	1.27	1.37	112.53	1
P38	00 42 37.74	41 16 43.0	-301.0	4.6	-0.24	1.34	1.36	100.09	1
P140	00 42 38.03	41 13 44.1	-288.2	4.6	-2.65	-0.41	2.68	188.82	1
P437	00 42 38.13	41 9 55.1	-474.2	4.6	-5.77	-2.61	6.33	204.39	1
P35	00 42 38.27	41 15 33.3	-374.0	4.6	-1.13	0.60	1.28	152.28	1
P438	00 42 38.34	41 9 58.5	-483.2	4.6	-5.70	-2.61	6.27	204.65	1
P143	00 42 38.35	41 14 27.2	-267.5	4.6	-2.03	-0.05	2.03	181.37	1
P55	00 42 38.38	41 14 34.2	-492.9	4.6	-1.93	0.01	1.93	179.59	1
P439	00 42 38.53	41 11 17.5	-369.0	4.6	-4.60	-1.89	4.97	202.33	1
P102	00 42 39.53	41 18 31.1	-257.8	3.7	1.43	2.10	2.54	55.75	2
P82	00 42 39.80	41 17 3.0	-207.6	6.4	0.26	1.22	1.24	78.10	1

Table A1: Positions and Velocities of Planetary Nebulae.

P103	00 42 40.19	41 18 41.6	-359.4	4.6	1.64	2.10	2.67	51.93	1
PN_3_4_7	00 42 40.21	40 51 2.3	-147.5	8.2	-21.01	-13.76	25.12	213.22	1
P160	00 42 40.24	41 13 50.6	-199.6	6.4	-2.32	-0.69	2.42	196.53	1
PN_6_4_16	00 42 40.25	41 19 5.5	-744.8	13.5	1.98	2.32	3.05	49.54	1
P444	00 42 40.39	41 11 33.2	-444.0	4.6	-4.18	-2.03	4.65	205.84	1
P56	00 42 40.70	41 14 9.7	-253.2	4.6	-2.01	-0.58	2.09	196.01	1
P105	00 42 41.23	41 19 8.4	-142.2	6.4	2.12	2.20	3.05	45.97	1
P447	00 42 41.31	41 18 20.5	-334.9	6.4	1.48	1.73	2.27	49.43	1
P83	00 42 41.36	41 17 48.8	-549.9	4.6	1.05	1.41	1.76	53.42	1
P448	00 42 41.44	41 18 11.8	-218.6	13.3	1.37	1.62	2.12	49.77	1
P153	00 42 41.50	41 9 58.5	-595.6	4.6	-5.36	-3.10	6.19	210.07	1
PN_10_4_2	00 42 41.99	41 56 56.1	-113.6	11.6	33.17	23.75	40.79	35.61	1
P57	00 42 42.11	41 14 9.1	-308.6	4.6	-1.87	-0.80	2.03	203.19	1
P5	00 42 42.34	41 15 53.1	-604.5	4.6	-0.42	0.16	0.45	159.60	1
P450	00 42 42.83	41 9 46.5	-363.0	4.6	-5.38	-3.42	6.37	212.47	1
P154	00 42 42.89	41 9 22.0	-348.3	4.6	-5.70	-3.67	6.78	212.72	1
P8	00 42 43.79	41 16 0.9	-251.9	6.4	-0.16	0.01	0.16	176.68	1
P155	00 42 43.84	41 10 46.3	-244.1	4.6	-4.45	-3.01	5.37	214.03	1
P451	00 42 43.88	41 8 60.0	-375.3	4.6	-5.90	-4.03	7.14	214.33	1
P157	00 42 44.94	41 12 11.0	-356.6	4.6	-3.18	-2.37	3.96	216.68	1
P107	00 42 45.44	41 19 18.2	-174.5	3.3	2.71	1.64	3.17	31.21	2
P109	00 42 45.45	41 19 57.1	-328.6	6.4	3.24	2.01	3.82	31.82	1
PN_3_3_5	00 42 45.60	40 59 21.3	-329.3	6.0	-13.61	-9.83	16.79	215.82	1
P2	00 42 45.97	41 16 24.1	-212.1	4.6	0.39	-0.10	0.40	345.00	1
P455	00 42 46.01	41 18 24.8	-198.5	4.5	2.04	1.04	2.29	27.06	2
P1	00 42 46.18	41 16 41.0	-492.0	4.6	0.64	0.02	0.64	2.21	1
P67	00 42 46.66	41 13 16.0	-414.3	4.6	-2.10	-2.01	2.91	223.69	1
P61	00 42 46.72	41 14 21.0	-185.2	4.6	-1.21	-1.40	1.85	229.11	1
P456	00 42 47.22	41 11 32.5	-307.5	6.4	-3.46	-3.09	4.63	221.75	1
P457	00 42 47.29	41 11 39.5	-498.8	8.2	-3.35	-3.03	4.52	222.09	1
P12	00 42 47.55	41 16 21.3	-337.1	4.6	0.52	-0.37	0.64	324.34	1
P458	00 42 47.58	41 11 27.1	-296.4	4.6	-3.49	-3.19	4.73	222.44	1
P165	00 42 47.58	41 14 59.3	-524.7	6.4	-0.59	-1.16	1.31	242.94	1
P459	00 42 47.62	41 21 1.1	-169.9	13.3	4.35	2.29	4.92	27.77	1
P163	00 42 47.65	41 13 47.9	-146.2	4.6	-1.56	-1.86	2.43	229.94	1
P114	00 42 47.92	41 20 58.9	-150.9	4.6	4.35	2.22	4.89	27.06	1
P460	00 42 48.22	41 17 33.9	-492.0	6.4	1.59	0.22	1.60	7.79	1
P62	00 42 48.91	41 15 23.9	-565.7	4.6	-0.12	-1.13	1.14	264.20	1
P23	00 42 48.94	41 16 55.5	-111.2	3.3	1.14	-0.26	1.17	347.08	2
P227	00 42 49.44	41 22 10.3	-312.9	3.3	5.49	2.67	6.11	25.96	2
P330	00 42 49.58	41 16 49.9	-280.1	6.4	1.13	-0.41	1.20	339.93	1
P112	00 42 49.65	41 18 40.8	-165.9	4.6	2.65	0.64	2.73	13.49	1
P113	00 42 49.82	41 20 7.6	-269.3	4.6	3.86	1.44	4.12	20.48	1
PN_3_4_1	00 42 49.88	40 51 10.2	-525.7	11.6	-19.85	-15.18	24.99	217.41	1
PN_3_4_11	00 42 50.62	40 45 27.9	-183.3	6.0	-24.44	-18.57	30.70	217.23	1
P78	00 42 50.90	41 14 47.2	-338.4	4.6	-0.40	-1.79	1.83	257.37	1
P75	00 42 51.34	41 15 56.2	-400.4	6.4	0.59	-1.20	1.33	296.15	1
PN_10_4_1	00 42 51.78	41 58 46.2	-241.7	8.2	35.71	23.31	42.65	33.14	1
P28	00 42 52.11	41 17 24.4	-223.1	4.6	1.87	-0.47	1.93	345.85	1
P224	00 42 52.60	41 20 22.6	-201.0	3.7	4.36	1.16	4.51	14.86	2
P225	00 42 52.68	41 21 3.2	-243.1	4.6	4.92	1.53	5.16	17.29	1
P64	00 42 52.71	41 14 15.6	-601.8	4.6	-0.64	-2.37	2.46	254.95	1
P223	00 42 52.79	41 20 18.9	-206.1	4.6	4.33	1.09	4.47	14.15	1
PN_3_4_3	00 42 53.02	40 48 59.5	-207.5	6.0	-21.30	-16.92	27.20	218.47	1
PN_3_3_4	00 42 53.03	40 58 18.8	-346.9	8.2	-13.66	-11.57	17.90	220.27	1
P32	00 42 53.35	41 18 17.0	-120.3	4.6	2.73	-0.16	2.73	356.64	1
P24	00 42 53.37	41 16 27.9	-270.6	4.6	1.24	-1.21	1.73	315.77	1
P222	00 42 53.43	41 19 51.7	-211.7	4.6	4.03	0.73	4.09	10.32	1
P29	00 42 53.53	41 17 33.8	-450.4	4.6	2.16	-0.60	2.24	344.42	1
P475	00 42 54.17	41 13 36.7	-347.4	6.4	-1.01	-2.97	3.14	251.19	1

Table A1: Positions and Velocities of Planetary Nebulae.

P476	00 42 54.22	41 14 17.0	-133.9	4.6	-0.46	-2.59	2.63	260.03	1
PN_10_1_3	00 42 54.35	41 41 28.5	-260.8	13.5	21.83	13.00	25.40	30.77	1
P116	00 42 54.49	41 21 23.0	-351.8	3.3	5.39	1.44	5.58	15.00	2
P76	00 42 54.58	41 15 37.2	-115.5	4.6	0.68	-1.88	2.00	289.86	1
P77	00 42 54.59	41 15 21.6	-37.8	4.6	0.47	-2.03	2.08	282.95	1
P190	00 42 55.30	41 18 14.8	-240.3	4.6	2.91	-0.48	2.95	350.60	1
P30	00 42 55.44	41 17 20.7	-290.2	4.6	2.18	-1.02	2.41	334.95	1
P26	00 42 55.51	41 16 24.4	-421.1	13.3	1.42	-1.57	2.12	312.19	1
P479	00 42 55.69	41 25 49.1	-252.0	2.0	9.15	3.81	9.91	22.58	6
P175	00 42 55.79	41 16 15.8	-221.4	4.6	1.34	-1.69	2.16	308.24	1
P120	00 42 56.08	41 17 32.3	-241.3	4.6	2.41	-1.01	2.61	337.31	1
P122	00 42 56.20	41 19 12.7	-318.4	4.6	3.79	-0.07	3.79	359.01	1
P117	00 42 56.21	41 22 2.8	-8.4	3.3	6.12	1.56	6.31	14.31	2
PN_6_3_7	00 42 56.29	41 37 38.7	-541.0	13.5	18.90	10.50	21.62	29.06	1
P480	00 42 56.38	41 18 53.6	-139.5	8.2	3.55	-0.28	3.56	355.56	1
PN_6_3_8	00 42 56.38	41 29 41.4	-145.8	13.5	12.39	5.92	13.74	25.54	1
P167	00 42 56.39	41 13 28.7	-681.6	3.3	-0.88	-3.39	3.50	255.43	2
P171	00 42 56.92	41 14 8.4	-431.3	6.4	-0.28	-3.09	3.10	264.80	1
P191	00 42 56.93	41 18 14.1	-160.1	4.6	3.07	-0.74	3.16	346.49	1
P136	00 42 57.20	41 16 59.1	-332.6	4.6	2.08	-1.50	2.56	324.23	1
P80	00 42 57.33	41 17 25.4	-302.7	4.6	2.45	-1.27	2.76	332.69	1
P189	00 42 57.36	41 17 14.7	-524.7	4.6	2.31	-1.37	2.69	329.26	1
P232	00 42 57.43	41 23 5.5	-304.1	4.6	7.10	1.97	7.37	15.52	1
P33	00 42 57.75	41 18 47.9	129.6	4.6	3.62	-0.54	3.66	351.51	1
P27	00 42 57.98	41 16 21.3	-122.0	4.6	1.65	-1.98	2.57	309.76	1
P173	00 42 58.02	41 14 52.1	-430.8	4.6	0.43	-2.84	2.87	278.69	1
P31	00 42 58.33	41 17 9.7	-218.0	4.6	2.34	-1.57	2.82	326.20	1
P234	00 42 58.37	41 25 11.0	-403.4	6.4	8.92	3.03	9.42	18.76	1
P483	00 42 58.45	41 15 6.0	-524.7	8.2	0.67	-2.77	2.85	283.59	1
PN_3_3_10	00 42 58.47	40 59 34.6	-325.9	6.0	-12.04	-11.69	16.78	224.15	1
PN_6_4_54	00 42 58.87	41 22 13.2	-154.8	13.5	6.54	1.25	6.66	10.82	1
P180	00 42 58.95	41 18 54.5	30.5	4.6	3.84	-0.66	3.90	350.22	1
PN_10_4_10	00 42 59.10	42 2 14.0	-321.4	9.9	39.33	24.19	46.17	31.59	1
PN_10_1_7	00 42 59.26	41 48 40.0	-225.2	8.2	28.24	16.38	32.64	30.11	1
P221	00 42 59.35	41 21 45.9	-260.1	3.3	6.22	0.92	6.29	8.37	2
P484	00 42 59.58	41 20 3.0	69.8	6.4	4.84	-0.10	4.85	358.77	1
P231	00 42 59.64	41 23 7.9	-165.0	4.6	7.37	1.66	7.56	12.66	1
P135	00 42 59.92	41 16 49.0	-307.3	4.6	2.23	-2.01	3.01	317.98	1
P485	00 43 0.19	41 21 34.0	-291.3	6.4	6.15	0.67	6.19	6.25	1
PN_10_4_9	00 43 0.51	41 58 55.7	-283.9	8.2	36.77	22.08	42.89	30.98	1
P172	00 43 0.61	41 14 42.8	-252.2	4.6	0.59	-3.33	3.38	280.00	1
PN_6_3_11	00 43 0.81	41 30 11.5	-308.5	13.5	13.28	5.53	14.39	22.61	1
P124	00 43 0.86	41 18 42.4	-79.0	4.6	3.88	-1.07	4.03	344.57	1
P198	00 43 1.18	41 20 4.5	-220.1	4.6	5.04	-0.34	5.05	356.19	1
P487	00 43 1.31	41 26 20.1	-112.7	3.7	10.18	3.24	10.68	17.66	2
PN_3_4_12	00 43 2.04	40 49 30.0	-156.6	6.0	-19.90	-18.03	26.85	222.17	1
P177	00 43 2.39	41 16 49.6	-301.8	4.6	2.51	-2.39	3.46	316.43	1
P200	00 43 2.54	41 20 28.2	-253.5	3.7	5.51	-0.32	5.52	356.70	2
P489	00 43 2.56	41 16 59.9	-406.9	6.4	2.67	-2.31	3.53	319.06	1
PN_6_1_40	00 43 2.59	41 8 43.0	-344.7	13.5	-4.11	-7.08	8.18	239.85	1
P201	00 43 2.96	41 20 40.4	-148.9	3.3	5.72	-0.27	5.73	357.34	2
P491	00 43 3.00	41 26 10.8	-87.6	3.2	10.23	2.89	10.63	15.78	3
P235	00 43 3.53	41 24 35.3	-89.7	3.7	8.99	1.90	9.18	11.91	2
P179	00 43 3.72	41 17 37.3	-127.7	4.6	3.30	-2.13	3.93	327.12	1
P492	00 43 3.88	41 21 24.4	-314.0	4.6	6.42	0.01	6.42	0.13	1
P199	00 43 4.35	41 20 8.2	-243.7	4.6	5.43	-0.79	5.49	351.75	1
P493	00 43 4.56	41 14 43.1	-454.6	3.7	1.02	-3.93	4.06	284.50	2
P220	00 43 4.75	41 21 43.0	-144.7	4.6	6.77	0.06	6.77	0.50	1
PN_10_4_6	00 43 5.20	41 55 52.4	-288.4	6.0	34.77	19.61	39.92	29.42	1
P125	00 43 5.21	41 17 37.9	-225.5	3.3	3.47	-2.36	4.20	325.81	2

Table A1: Positions and Velocities of Planetary Nebulae.

P195	00 43 5.34	41 18 32.6	-549.7	4.6	4.23	-1.85	4.62	336.34	1
P132	00 43 5.39	41 19 28.2	-355.7	4.6	5.00	-1.33	5.17	345.10	1
P126	00 43 5.70	41 18 13.6	-525.1	4.6	4.01	-2.09	4.52	332.46	1
P130	00 43 5.91	41 19 15.7	-252.2	4.6	4.88	-1.53	5.12	342.60	1
P127	00 43 6.01	41 18 28.2	31.4	4.6	4.24	-2.00	4.69	334.78	1
P134	00 43 6.13	41 20 3.3	-48.0	4.6	5.55	-1.11	5.66	348.73	1
P205	00 43 6.15	41 20 19.4	-263.5	6.4	5.78	-0.96	5.86	350.60	1
PN_6_3_12	00 43 6.22	41 30 19.4	-221.3	11.6	13.97	4.78	14.76	18.88	1
P495	00 43 6.40	41 17 50.5	-302.5	6.4	3.77	-2.42	4.48	327.31	1
P128	00 43 6.62	41 18 37.5	-80.0	4.6	4.44	-2.00	4.87	335.69	1
P241	00 43 7.05	41 24 56.0	-112.7	3.3	9.65	1.55	9.77	9.15	2
P131	00 43 7.30	41 19 21.8	-338.2	4.6	5.11	-1.68	5.39	341.77	1
P497	00 43 7.89	41 15 47.1	-34.9	4.6	2.25	-3.83	4.44	300.42	1
P498	00 43 7.94	41 15 37.5	-99.3	6.4	2.12	-3.93	4.47	298.39	1
P499	00 43 8.15	41 17 42.0	-334.2	6.4	3.84	-2.77	4.74	324.22	1
P133	00 43 8.80	41 20 0.7	-366.3	4.6	5.81	-1.54	6.01	345.12	1
P129	00 43 9.05	41 18 43.8	-431.8	4.6	4.79	-2.32	5.32	334.16	1
P178	00 43 9.48	41 15 53.0	-218.1	3.3	2.50	-4.02	4.73	301.90	2
P254	00 43 9.78	41 26 51.9	-107.9	3.3	11.52	2.24	11.74	11.02	2
PN_6_4_65	00 43 9.86	41 27 7.1	-320.3	13.5	11.74	2.38	11.98	11.45	1
PN_10_3_2	00 43 10.51	42 11 33.2	-291.2	13.5	48.17	27.81	55.62	30.00	1
P240	00 43 10.82	41 25 40.3	-94.5	3.1	10.66	1.40	10.75	7.48	3
P203	00 43 10.78	41 19 53.5	-107.4	4.6	5.92	-1.92	6.22	342.08	1
PN_10_3_1	00 43 11.58	42 7 12.7	-209.1	5.3	44.73	25.15	51.32	29.35	1
P239	00 43 12.36	41 25 26.0	-60.5	4.6	10.63	1.03	10.68	5.51	1
PN_6_1_44	00 43 12.41	41 12 43.5	-343.3	8.2	0.23	-6.28	6.29	272.13	1
P501	00 43 12.43	41 23 46.7	-288.2	4.5	9.28	0.06	9.28	0.40	2
P219	00 43 12.53	41 21 16.7	-140.3	4.6	7.25	-1.39	7.38	349.16	1
P502	00 43 12.89	41 16 43.4	-224.4	3.7	3.56	-4.06	5.40	311.22	2
P206	00 43 12.93	41 18 49.3	-125.4	4.6	5.28	-2.86	6.00	331.54	1
P237	00 43 13.22	41 24 22.2	-68.4	4.6	9.85	0.28	9.85	1.65	1
PN_3_4_13	00 43 13.73	40 52 32.2	-407.8	6.0	-16.14	-18.09	24.25	228.25	1
P218	00 43 14.12	41 21 12.6	-309.1	4.4	7.36	-1.67	7.55	347.21	2
P242	00 43 14.37	41 21 59.9	-343.7	4.6	8.03	-1.26	8.13	351.11	1
PN_3_3_14	00 43 15.21	41 4 21.3	-389.1	13.5	-6.31	-11.53	13.14	241.29	1
P504	00 43 15.32	41 18 27.9	-573.5	4.6	5.25	-3.43	6.27	326.79	1
P207	00 43 15.65	41 18 0.7	-371.5	4.6	4.91	-3.74	6.17	322.67	1
P212	00 43 15.79	41 19 25.8	-108.9	4.6	6.09	-2.95	6.76	334.13	1
P253	00 43 16.22	41 27 4.5	-96.9	2.5	12.39	1.38	12.46	6.35	4
P214	00 43 16.65	41 19 46.1	-146.1	6.4	6.45	-2.89	7.07	335.89	1
P252	00 43 16.71	41 26 27.6	-194.3	4.6	11.94	0.95	11.97	4.55	1
P243	00 43 16.72	41 22 26.2	-43.9	4.6	8.65	-1.37	8.75	351.03	1
P211	00 43 17.24	41 19 33.1	-78.7	4.6	6.34	-3.10	7.06	333.92	1
P213	00 43 17.98	41 19 43.2	-79.2	4.6	6.56	-3.12	7.26	334.56	1
P217	00 43 17.99	41 21 34.5	-245.2	3.3	8.08	-2.06	8.34	345.72	2
PN_10_1_11	00 43 18.00	41 45 46.4	-232.8	6.0	27.88	11.85	30.29	23.04	1
P210	00 43 18.13	41 19 34.9	-288.1	4.6	6.46	-3.22	7.22	333.49	1
PN_10_1_14	00 43 18.26	41 43 35.3	-228.0	6.0	26.12	10.56	28.17	22.01	1
P505	00 43 18.68	41 15 39.5	-88.6	2.6	3.31	-5.56	6.47	300.76	4
PN_6_1_46	00 43 19.21	41 12 12.9	-295.9	13.5	0.55	-7.62	7.64	274.14	1
P208	00 43 19.41	41 17 45.8	12.2	4.6	5.11	-4.47	6.79	318.87	1
PN_3_3_17	00 43 19.85	41 2 33.9	-418.9	6.0	-7.27	-13.27	15.13	241.27	1
PN_3_3_22	00 43 20.61	40 55 32.3	-310.9	6.0	-12.94	-17.43	21.71	233.41	1
PN_3_3_21	00 43 20.66	40 57 44.0	-518.8	6.0	-11.14	-16.17	19.64	235.44	1
P209	00 43 20.85	41 17 51.4	-322.4	2.7	5.34	-4.63	7.07	319.08	3
PN_3_3_18	00 43 21.34	41 5 28.7	-375.8	6.0	-4.73	-11.83	12.74	248.20	1
P244	00 43 23.43	41 23 51.3	-304.0	4.6	10.53	-1.58	10.65	351.47	1
PN_10_4_15	00 43 23.54	41 53 36.0	-300.6	6.0	34.87	15.51	38.17	23.98	1
PN_6_3_21	00 43 23.64	41 36 11.2	-188.9	13.5	20.64	5.48	21.36	14.87	1
PN_10_1_8	00 43 23.70	41 50 18.7	-207.7	6.0	32.20	13.59	34.95	22.89	1

Table A1: Positions and Velocities of Planetary Nebulae.

P251	00 43 24.31	41 24 37.4	-55.3	4.6	11.25	-1.27	11.33	353.55	1
P246	00 43 24.31	41 23 16.0	-85.4	4.6	10.14	-2.05	10.35	348.56	1
P245	00 43 24.57	41 23 44.1	6.9	4.6	10.55	-1.82	10.71	350.20	1
P511	00 43 24.69	41 20 24.4	-297.8	6.4	7.85	-3.76	8.70	334.42	1
P250	00 43 24.78	41 24 48.5	-121.2	4.6	11.46	-1.24	11.52	353.83	1
P512	00 43 25.82	41 22 40.7	-302.9	4.6	9.83	-2.62	10.17	345.05	1
P34	00 43 26.16	41 25 54.0	-105.7	6.4	12.50	-0.82	12.52	356.24	1
PN_6_3_28	00 43 26.19	41 29 37.3	-51.8	8.2	15.54	1.31	15.60	4.83	1
PN_6_1_64	00 43 26.43	41 6 42.3	-343.4	13.5	-3.17	-11.90	12.32	255.07	1
P216	00 43 26.59	41 20 26.3	-231.3	4.6	8.08	-4.03	9.03	333.48	1
PN_6_1_57	00 43 27.07	41 10 28.2	-260.8	8.2	-0.03	-9.84	9.84	269.85	1
PN_10_3_6	00 43 27.24	42 4 45.6	-201.3	4.8	44.40	21.37	49.27	25.70	2
PN_6_4_93	00 43 28.48	41 20 17.8	-261.2	9.9	8.16	-4.40	9.28	331.67	1
PN_10_4_17	00 43 28.49	41 51 55.3	-149.5	6.0	34.03	13.79	36.72	22.06	1
PN_10_3_4	00 43 28.80	42 11 6.4	-124.8	11.6	49.76	24.78	55.59	26.48	1
PN_10_4_11	00 43 32.36	41 58 42.4	-611.7	6.0	39.99	17.11	43.50	23.16	1
P279	00 43 32.67	41 26 16.8	-177.0	4.6	13.51	-1.60	13.60	353.24	1
PN_10_4_13	00 43 32.82	41 54 9.9	-333.4	6.0	36.33	14.42	39.09	21.65	1
PN_10_4_16	00 43 33.16	41 52 45.5	-244.2	6.0	35.22	13.56	37.74	21.06	1
P270	00 43 33.37	41 27 50.0	-165.8	6.4	14.86	-0.81	14.88	356.86	1
P518	00 43 35.41	41 22 30.0	-90.2	4.6	10.71	-4.20	11.51	338.61	1
PN_10_1_15	00 43 36.30	41 42 57.0	-125.0	8.2	27.53	7.44	28.52	15.12	1
PN_10_1_17	00 43 36.60	41 49 42.8	-227.6	6.0	33.09	11.29	34.97	18.83	1
PN_3_3_24	00 43 36.81	41 3 32.6	-279.4	8.2	-4.64	-15.32	16.01	253.17	1
PN_3_1_2	00 43 36.84	40 37 38.0	-323.2	4.2	-25.82	-30.24	39.76	229.51	2
PN_6_3_36	00 43 37.22	41 31 4.7	-658.0	6.0	17.92	0.46	17.93	1.48	1
P520	00 43 37.27	41 22 38.0	-263.5	3.3	11.02	-4.41	11.87	338.22	2
PN_6_1_61	00 43 37.35	41 14 30.0	-253.3	8.2	4.38	-9.10	10.10	295.72	1
P275	00 43 37.90	41 27 38.9	-113.8	3.3	15.19	-1.62	15.28	353.93	2
P281	00 43 38.03	41 24 33.7	-166.1	3.3	12.68	-3.41	13.13	344.94	2
P282	00 43 38.27	41 24 5.5	-242.6	4.6	12.33	-3.72	12.87	343.21	1
PN_10_1_18	00 43 38.71	41 49 31.0	-191.6	8.2	33.16	10.85	34.89	18.12	1
P278	00 43 39.26	41 26 29.8	-132.7	3.7	14.40	-2.49	14.61	350.20	2
P276	00 43 39.34	41 26 53.4	-212.9	4.6	14.73	-2.27	14.90	351.23	1
P522	00 43 39.40	41 22 57.6	-64.5	4.6	11.52	-4.54	12.39	338.48	1
PN_6_3_47	00 43 40.12	41 35 4.6	-168.2	9.9	21.51	2.32	21.63	6.16	1
P283	00 43 40.61	41 23 30.1	-167.9	4.6	12.10	-4.42	12.88	339.93	1
PN_6_4_110	00 43 41.37	41 18 11.5	-276.3	6.0	7.84	-7.59	10.91	315.90	1
P274	00 43 41.74	41 28 2.8	-191.1	4.6	15.93	-1.97	16.05	352.94	1
P523	00 43 42.47	41 22 47.1	-395.5	4.6	11.71	-5.12	12.78	336.40	1
PN_6_1_66	00 43 43.28	41 9 30.9	-348.3	8.2	0.95	-12.88	12.92	274.21	1
P285	00 43 43.39	41 27 31.0	-4.6	4.6	15.68	-2.53	15.88	350.83	1
PN_6_1_68	00 43 43.94	41 11 36.5	-303.3	11.6	2.73	-11.78	12.09	283.06	1
PN_3_3_23	00 43 44.52	40 59 59.4	-279.7	6.0	-6.70	-18.56	19.73	250.14	1
P284	00 43 44.99	41 27 14.5	-171.8	4.6	15.63	-2.94	15.90	349.36	1
PN_6_3_48	00 43 45.18	41 35 17.9	-558.6	13.5	22.23	1.68	22.30	4.31	1
P525	00 43 45.23	41 23 55.3	-145.4	4.6	12.94	-4.88	13.83	339.32	1
PN_3_4_20	00 43 47.43	40 47 19.0	-466.7	6.0	-16.75	-26.31	31.19	237.52	1
PN_6_3_45	00 43 48.20	41 31 26.3	6.9	6.0	19.40	-1.01	19.43	357.02	1
PN_6_3_52	00 43 49.67	41 38 7.5	-538.9	13.5	25.03	2.62	25.16	5.97	1
P286	00 43 49.72	41 27 58.4	-13.0	4.6	16.73	-3.24	17.04	349.05	1
PN_10_4_19	00 43 51.05	41 58 24.6	-68.7	6.0	41.75	14.10	44.07	18.65	1
PN_3_3_27	00 43 52.63	40 57 38.8	-402.6	6.0	-7.74	-21.16	22.53	249.92	1
PN_3_3_26	00 43 53.08	40 55 9.9	-405.8	6.0	-9.72	-22.66	24.65	246.79	1
PN_10_4_20	00 43 54.17	42 2 39.0	-231.0	6.0	45.55	16.07	48.30	19.43	1
PN_6_3_58	00 43 54.74	41 35 2.3	-91.8	13.5	23.05	0.07	23.05	0.16	1
PN_10_1_16	00 43 54.89	41 45 39.2	-230.2	6.0	31.74	6.16	32.33	10.98	1
PN_10_1_27	00 43 54.93	41 43 51.7	-499.2	6.0	30.28	5.12	30.71	9.60	1
P288	00 43 55.05	41 26 4.9	-155.1	4.6	15.76	-5.14	16.58	341.93	1
P529	00 43 58.21	41 30 44.9	-6.8	6.4	19.92	-2.94	20.13	351.61	1

Table A1: Positions and Velocities of Planetary Nebulae.

P530	00 43 58.63	41 27 18.5	-126.9	4.4	17.15	-4.99	17.86	343.79	2
PN_6_1_72	00 43 58.85	41 11 30.1	-247.3	8.2	4.26	-14.13	14.76	286.78	1
PN_6_1_73	00 43 59.45	41 16 47.4	-30.5	6.0	8.65	-11.18	14.13	307.73	1
PN_6_1_74	00 43 59.92	41 15 35.2	-255.5	6.0	7.71	-11.94	14.22	302.86	1
PN_10_1_31	00 43 59.95	41 50 56.8	-40.1	6.0	36.61	8.44	37.57	12.98	1
PN_10_1_26	00 44 0.34	41 43 56.8	-116.3	6.0	30.93	4.35	31.24	8.00	1
PN_10_1_30	00 44 1.35	41 47 8.2	-181.0	6.0	33.65	6.03	34.18	10.16	1
P532	00 44 2.48	41 28 3.1	-40.3	6.4	18.18	-5.15	18.89	344.19	1
P533	00 44 2.86	41 31 16.7	-100.2	3.3	20.85	-3.34	21.12	350.89	2
PN_6_3_57	00 44 3.89	41 36 52.3	-35.9	8.2	25.53	-0.28	25.54	359.38	1
P536	00 44 6.70	41 28 5.4	-72.9	6.4	18.66	-5.77	19.53	342.82	1
P537	00 44 7.18	41 25 31.3	-152.1	6.4	16.62	-7.33	18.16	336.21	1
PN_6_1_75	00 44 7.51	41 10 9.3	-272.2	8.2	4.10	-16.24	16.75	284.17	1
P538	00 44 7.68	41 30 40.3	-149.1	6.4	20.88	-4.43	21.34	348.02	1
P539	00 44 8.13	41 31 18.7	-187.4	4.6	21.45	-4.13	21.84	349.10	1
PN_6_1_95	00 44 8.83	41 15 20.4	-223.3	8.2	8.48	-13.45	15.90	302.22	1
P541	00 44 9.52	41 27 11.6	-124.5	4.4	18.24	-6.72	19.43	339.77	2
PN_10_3_7	00 44 9.93	42 6 40.1	-106.1	4.8	50.52	15.99	52.99	17.57	2
PN_10_4_21	00 44 10.84	41 56 29.4	-68.4	6.0	42.31	9.98	43.47	13.28	1
PN_6_3_70	00 44 11.27	41 34 24.3	-107.1	8.2	24.31	-2.83	24.48	353.37	1
PN_3_3_28	00 44 11.42	41 1 1.8	-349.3	4.2	-2.93	-22.11	22.30	262.46	2
PN_6_1_70	00 44 11.94	41 13 59.8	-234.9	6.0	7.72	-14.70	16.61	297.70	1
PN_10_4_23	00 44 12.01	41 54 11.2	-149.4	6.0	40.55	8.48	41.43	11.81	1
PN_6_3_85	00 44 12.15	41 39 49.1	-620.8	11.6	28.83	0.16	28.83	0.32	1
PN_10_1_24	00 44 12.48	41 44 19.4	-198.8	6.0	32.55	2.71	32.66	4.76	1
P545	00 44 13.15	41 30 9.5	-314.9	4.6	21.05	-5.56	21.77	345.19	1
PN_6_3_68	00 44 13.48	41 31 53.8	-21.9	6.0	22.50	-4.61	22.97	348.42	1
P548	00 44 15.46	41 27 15.1	-177.9	8.2	18.93	-7.59	20.39	338.14	1
PN_6_3_81	00 44 15.71	41 34 21.2	-131.9	11.6	24.75	-3.53	25.00	351.87	1
P549	00 44 16.17	41 31 18.4	-101.4	6.4	22.31	-5.36	22.95	346.49	1
PN_10_4_27	00 44 16.23	41 57 3.1	-225.1	6.0	43.34	9.49	44.37	12.35	1
PN_10_1_36	00 44 16.29	41 42 22.3	-136.5	8.2	31.36	1.01	31.38	1.84	1
P550	00 44 17.03	41 29 48.1	-48.2	4.6	21.18	-6.36	22.11	343.28	1
P551	00 44 17.68	41 33 42.5	-147.8	4.6	24.44	-4.21	24.80	350.23	1
PN_10_1_32	00 44 19.33	41 46 9.0	-82.5	6.0	34.77	2.72	34.88	4.48	1
P554	00 44 19.65	41 30 20.7	-209.6	13.3	21.90	-6.45	22.83	343.59	1
PN_3_4_21	00 44 20.37	40 49 4.7	-277.6	6.0	-11.71	-30.38	32.56	248.92	1
PN_6_4_151	00 44 20.88	41 24 26.8	-201.9	6.0	17.22	-10.04	19.94	329.75	1
PN_6_3_83	00 44 22.38	41 35 51.5	-4.9	6.0	26.70	-3.68	26.95	352.15	1
PN_10_4_30	00 44 23.35	41 53 35.7	-114.7	6.0	41.28	6.41	41.78	8.83	1
PN_10_1_37	00 44 23.60	41 40 49.1	1.4	8.2	30.88	-1.01	30.90	358.14	1
PN_6_4_147	00 44 23.70	41 25 51.7	-275.4	8.2	18.68	-9.66	21.03	332.66	1
PN_10_4_29	00 44 24.08	41 55 26.5	-154.6	8.2	42.87	7.37	43.50	9.75	1
P555	00 44 24.41	41 29 46.4	-102.5	4.6	21.95	-7.51	23.20	341.12	1
PN_6_3_88	00 44 24.95	41 38 30.5	-181.6	6.0	29.14	-2.55	29.25	355.01	1
P557	00 44 24.96	41 31 45.7	-72.9	4.6	23.63	-6.44	24.50	344.75	1
PN_10_1_33	00 44 25.12	41 42 45.3	-88.3	6.0	32.63	-0.12	32.63	359.79	1
P558	00 44 25.42	41 29 52.9	-136.1	4.6	22.15	-7.60	23.42	341.06	1
PN_6_4_149	00 44 25.63	41 26 40.4	-331.3	6.0	19.55	-9.48	21.73	334.12	1
PN_10_4_25	00 44 25.75	41 59 56.9	-161.6	6.0	46.73	9.72	47.73	11.75	1
PN_9_2_42	00 44 25.96	42 2 1.8	-157.7	6.0	48.45	10.89	49.66	12.66	1
PN_10_4_31	00 44 26.06	41 52 7.4	-137.4	11.6	40.37	5.15	40.70	7.27	1
P559	00 44 26.33	41 33 15.0	-117.6	3.7	25.00	-5.79	25.66	346.95	2
PN_6_4_154	00 44 27.55	41 22 28.6	-254.9	6.0	16.34	-12.20	20.39	323.24	1
PN_6_4_153	00 44 28.32	41 23 17.5	-366.8	6.0	17.08	-11.85	20.79	325.26	1
PN_10_4_28	00 44 28.79	41 56 59.6	-122.9	8.2	44.64	7.55	45.28	9.60	1
P560	00 44 29.82	41 32 45.1	-195.5	4.6	24.97	-6.61	25.83	345.16	1
P561	00 44 30.18	41 32 35.7	-203.6	6.4	24.88	-6.76	25.78	344.80	1
PN_10_3_8	00 44 30.49	42 8 55.1	-90.1	4.2	54.56	14.18	56.37	14.57	2
P562	00 44 30.97	41 33 41.7	-78.2	4.0	25.86	-6.24	26.61	346.43	1

Table A1: Positions and Velocities of Planetary Nebulae.

PN_6_4_157	00 44 31.43	41 21 31.2	-249.3	6.0	15.98	-13.35	20.82	320.12	1
PN_6_4_152	00 44 32.19	41 25 47.1	-120.5	6.0	19.54	-11.00	22.42	330.62	1
PN_10_1_43	00 44 32.44	41 46 37.8	-12.5	6.0	36.58	1.01	36.59	1.58	1
P563	00 44 34.56	41 33 29.4	-161.8	4.6	26.08	-6.91	26.98	345.16	1
PN_6_3_95	00 44 34.66	41 29 16.8	-185.0	6.0	22.66	-9.36	24.52	337.56	1
PN_5_2_5	00 44 35.12	41 8 4.7	-336.3	13.5	5.41	-21.68	22.35	284.00	1
PN_10_4_33	00 44 35.60	41 56 6.9	-105.4	6.0	44.66	6.01	45.06	7.66	1
PN_9_2_32	00 44 37.56	41 50 43.7	-154.7	6.0	40.47	2.60	40.56	3.67	1
PN_10_1_38	00 44 38.25	41 43 53.9	-138.6	8.2	34.97	-1.46	35.01	357.61	1
PN_10_4_32	00 44 38.57	41 53 2.2	-153.4	6.0	42.47	3.78	42.63	5.08	1
P564	00 44 38.82	41 31 31.3	-153.7	4.6	24.94	-8.70	26.41	340.77	1
PN_5_3_3	00 44 40.98	41 37 6.7	-177.3	5.5	29.73	-5.80	30.29	348.97	2
P566	00 44 41.71	41 32 4.1	-206.2	2.3	25.70	-8.82	27.17	341.05	4
PN_5_1_5	00 44 42.22	41 8 1.4	-255.9	6.0	6.13	-22.81	23.62	285.05	1
PN_4_1_1	00 44 42.76	40 40 5.5	-386.6	4.2	-16.60	-39.04	42.42	246.97	2
PN_5_1_2	00 44 43.79	41 14 27.8	-320.6	4.2	11.56	-19.32	22.52	300.89	2
PN_9_1_5	00 44 44.61	41 47 5.8	-383.4	6.0	38.27	-0.58	38.27	359.14	1
PN_9_1_14	00 44 45.03	41 41 56.3	-59.2	6.0	34.11	-3.62	34.30	353.94	1
P567	00 44 45.24	41 31 49.6	-190.7	4.6	25.88	-9.50	27.57	339.84	1
PN_9_1_4	00 44 48.49	41 48 17.7	-150.5	6.0	39.67	-0.47	39.67	359.32	1
PN_5_3_2	00 44 49.77	41 39 16.2	-153.3	5.8	32.44	-5.89	32.97	349.71	2
P568	00 44 50.13	41 31 7.9	-118.5	4.6	25.84	-10.65	27.95	337.60	1
P569	00 44 50.32	41 31 50.9	-159.3	2.7	26.45	-10.27	28.37	338.79	3
PN_9_3_2	00 44 52.26	42 11 57.5	-41.6	6.0	59.37	12.65	60.70	12.02	1
PN_9_1_3	00 44 52.77	41 49 44.2	-191.3	6.0	41.30	-0.29	41.30	359.60	1
PN_5_1_3	00 44 53.09	41 15 58.1	-226.4	8.2	13.80	-19.88	24.20	304.77	1
PN_9_4_3	00 44 53.63	41 53 25.3	-120.1	6.0	44.40	1.71	44.43	2.21	1
PN_9_1_12	00 44 53.80	41 42 23.0	-74.8	6.0	35.42	-4.70	35.73	352.44	1
PN_5_3_1	00 44 54.06	41 35 8.8	-238.9	6.0	29.54	-8.93	30.86	343.19	1
PN_4_4_1	00 44 54.41	40 52 45.2	-463.7	4.2	-4.99	-33.51	33.88	261.53	2
PN_9_4_6	00 44 54.70	41 53 5.5	18.3	6.0	44.25	1.36	44.27	1.76	1
PN_9_4_1	00 44 54.71	42 0 37.4	-689.6	13.5	50.39	5.72	50.71	6.47	1
PN_5_1_4	00 44 54.99	41 9 52.8	-330.2	4.2	9.04	-23.69	25.36	290.88	2
PN_5_4_2	00 44 55.97	41 23 24.1	-233.2	9.9	20.17	-16.02	25.76	321.55	1
PN_5_4_3	00 44 56.30	41 20 25.2	-298.2	4.2	17.78	-17.79	25.15	314.97	2
PN_9_4_4	00 44 56.94	41 54 29.5	-74.6	6.0	45.63	1.83	45.67	2.30	1
PN_5_4_1	00 44 57.06	41 26 16.9	-170.2	8.2	22.64	-14.52	26.89	327.33	1
PN_9_1_9	00 44 57.42	41 45 57.9	-170.7	6.0	38.73	-3.18	38.86	355.31	1
PN_9_3_4	00 44 59.86	42 7 44.7	-194.3	6.0	56.75	9.06	57.47	9.07	1
PN_5_4_7	00 45 2.95	41 25 27.6	-258.5	6.0	22.61	-15.89	27.64	324.90	1
PN_5_3_13	00 45 3.26	41 35 52.0	-96.7	6.0	31.13	-9.91	32.67	342.33	1
PN_9_4_11	00 45 3.37	41 58 16.7	-126.7	6.0	49.41	3.05	49.50	3.53	1
PN_9_4_9	00 45 3.51	41 59 49.5	-207.6	8.2	50.68	3.92	50.84	4.42	1
PN_5_3_12	00 45 3.72	41 32 38.5	-152.6	8.2	28.55	-11.85	30.91	337.45	1
PN_9_1_6	00 45 4.01	41 46 7.2	-101.7	6.0	39.57	-4.09	39.78	354.10	1
PN_5_1_7	00 45 5.06	41 12 52.1	-215.7	4.2	12.57	-23.51	26.66	298.14	2
PN_5_1_6	00 45 5.30	41 9 38.2	-291.1	6.0	9.96	-25.41	27.30	291.41	1
PN_5_3_16	00 45 6.08	41 36 16.3	-126.7	6.0	31.76	-10.11	33.33	342.34	1
PN_5_4_5	00 45 6.68	41 23 35.5	-204.6	6.0	21.49	-17.54	27.74	320.77	1
PN_4_1_2	00 45 6.82	40 32 10.5	-272.4	4.2	-20.41	-47.34	51.55	246.68	2
PN_4_1_3	00 45 7.14	40 39 33.3	-284.0	4.2	-14.36	-43.12	45.45	251.58	2
PN_5_4_8	00 45 7.34	41 25 28.6	-189.8	9.9	23.10	-16.55	28.42	324.37	1
PN_5_3_14	00 45 9.47	41 34 30.2	-138.1	6.0	30.69	-11.65	32.82	339.21	1
PN_9_1_20	00 45 11.72	41 47 39.6	-135.6	6.0	41.65	-4.37	41.88	354.01	1
PN_9_1_21	00 45 12.50	41 47 45.0	-92.5	6.0	41.81	-4.44	42.05	353.94	1
PN_9_3_9	00 45 14.34	42 11 56.8	-138.7	8.2	61.73	9.31	62.43	8.57	1
PN_5_3_19	00 45 14.45	41 39 3.1	-105.5	6.0	34.93	-9.77	36.28	344.37	1
PN_9_3_8	00 45 15.08	42 5 58.6	-6.2	6.0	56.94	5.73	57.23	5.75	1
PN_5_4_4	00 45 16.26	41 18 14.1	-286.9	6.0	18.17	-22.11	28.62	309.40	1
PN_9_1_22	00 45 17.07	41 49 53.7	-83.1	6.0	44.05	-3.89	44.22	354.96	1

Table A1: Positions and Velocities of Planetary Nebulae.

PN_9_4_8	00 45 17.73	42 2 26.7	-115.1	8.2	54.35	3.29	54.45	3.46	1
PN_9_4_7	00 45 17.93	41 56 49.2	-226.3	6.0	49.79	0.00	49.79	360.00	1
PN_9_3_10	00 45 18.96	42 12 44.7	-185.0	8.2	62.87	9.07	63.53	8.21	1
PN_9_4_16	00 45 21.07	41 52 7.8	-44.8	6.0	46.31	-3.20	46.42	356.05	1
PN_5_4_9	00 45 21.53	41 25 57.2	-189.4	6.0	25.03	-18.45	31.09	323.61	1
PN_9_4_13	00 45 23.00	42 0 38.7	-155.6	8.2	53.45	1.45	53.47	1.55	1
PN_5_3_25	00 45 23.64	41 35 50.5	-167.0	6.0	33.31	-13.03	35.77	338.63	1
PN_9_4_17	00 45 24.28	41 52 0.1	-70.1	6.0	46.55	-3.76	46.70	355.38	1
PN_9_1_19	00 45 24.85	41 47 31.4	-95.6	6.0	42.96	-6.44	43.44	351.47	1
PN_9_3_11	00 45 25.48	42 14 10.6	-146.9	13.5	64.74	8.92	65.35	7.84	1
PN_9_3_13	00 45 26.65	42 8 33.8	-548.8	8.2	60.29	5.49	60.54	5.20	1
PN_5_3_27	00 45 26.97	41 32 9.3	-87.9	6.0	30.67	-15.68	34.45	332.92	1
PN_5_3_28	00 45 27.00	41 30 13.3	-235.7	6.0	29.10	-16.81	33.60	329.99	1
PN_9_1_29	00 45 27.07	41 41 17.9	-127.0	6.0	38.13	-10.39	39.52	344.76	1
PN_9_4_18	00 45 27.68	41 55 40.5	-137.9	6.0	49.91	-2.15	49.95	357.54	1
PN_5_3_22	00 45 28.10	41 34 34.5	-187.8	8.2	32.77	-14.45	35.81	336.21	1
PN_9_4_19	00 45 29.07	41 55 47.7	-218.8	6.0	50.15	-2.29	50.21	357.39	1
PN_9_3_14	00 45 31.55	42 8 38.6	-279.3	6.0	60.89	4.79	61.07	4.50	1
PN_4_4_2	00 45 32.80	40 53 36.6	-157.5	6.0	-0.09	-38.93	38.93	269.87	1
PN_4_3_4	00 45 35.33	40 59 56.7	-214.4	6.0	5.35	-35.64	36.04	278.53	1
PN_9_1_26	00 45 36.85	41 47 20.4	-70.0	6.0	44.11	-8.37	44.90	349.25	1
PN_9_4_14	00 45 38.44	42 0 24.3	-126.9	8.2	54.92	-1.03	54.93	358.93	1
PN_9_1_31	00 45 38.65	41 40 36.8	-220.4	11.6	38.83	-12.55	40.80	342.09	1
PN_9_1_32	00 45 41.57	41 43 6.4	-210.2	6.0	41.17	-11.55	42.76	344.34	1
PN_9_1_28	00 45 42.30	41 44 28.9	-183.9	6.0	42.37	-10.86	43.74	345.63	1
PN_9_4_25	00 45 42.67	41 52 7.6	-554.5	6.0	48.64	-6.48	49.07	352.42	1
PN_9_4_27	00 45 42.94	41 58 19.8	6.4	6.0	53.72	-2.92	53.79	356.89	1
PN_9_3_16	00 45 43.61	42 9 24.6	-352.1	5.3	62.81	3.42	62.90	3.11	2
PN_5_4_10	00 45 43.98	41 22 40.3	-325.1	4.2	24.80	-23.78	34.36	316.20	2
PN_5_4_11	00 45 44.85	41 24 29.5	-142.1	6.0	26.37	-22.85	34.90	319.09	1
PN_9_1_24	00 45 45.87	41 49 44.2	-216.3	6.0	47.04	-8.35	47.77	349.93	1
PN_9_3_17	00 45 46.03	42 3 33.7	-121.0	6.0	58.31	-0.34	58.31	359.66	1
PN_9_4_29	00 45 46.22	41 59 42.3	-98.3	8.2	55.19	-2.61	55.25	357.29	1
PN_5_4_12	00 45 47.63	41 25 22.6	-245.0	9.9	27.40	-22.76	35.62	320.28	1
PN_5_1_9	00 45 47.67	41 9 17.4	-117.3	13.5	14.31	-32.11	35.16	294.01	1
PN_9_4_28	00 45 49.08	41 59 38.2	-122.3	6.0	55.44	-3.09	55.53	356.81	1
PN_5_3_33	00 45 49.19	41 36 44.1	-166.4	11.6	36.81	-16.40	40.30	335.98	1
PN_9_3_18	00 45 52.14	42 4 5.2	-1.9	9.9	59.39	-0.96	59.40	359.07	1
PN_9_4_32	00 45 52.42	42 2 13.0	-123.9	6.0	57.90	-2.09	57.94	357.93	1
PN_9_3_19	00 45 53.36	42 8 50.4	-66.0	11.6	63.39	1.61	63.41	1.46	1
PN_5_3_30	00 45 53.79	41 35 34.7	-119.3	4.2	36.37	-17.78	40.48	333.95	2
PN_9_1_33	00 45 56.03	41 43 16.4	-183.9	6.0	42.88	-13.65	45.00	342.35	1
PN_5_1_10	00 45 56.20	41 12 14.4	-213.9	8.2	17.64	-31.71	36.28	299.09	1
PN_9_3_21	00 45 57.21	42 7 45.8	-92.0	8.2	62.93	0.41	62.93	0.37	1
PN_9_1_36	00 46 0.28	41 45 46.8	-103.1	6.0	45.38	-12.83	47.16	344.21	1
PN_5_3_32	00 46 0.58	41 39 25.9	-144.9	6.0	40.24	-16.57	43.52	337.62	1
PN_9_1_37	00 46 1.89	41 49 47.1	-70.5	6.0	48.81	-10.75	49.98	347.58	1
PN_5_3_34	00 46 2.01	41 31 40.5	-123.8	4.8	34.09	-21.30	40.19	328.00	2
PN_9_4_33	00 46 4.87	41 56 38.0	-117.0	6.0	54.70	-7.22	55.18	352.48	1
PN_9_3_23	00 46 6.22	42 7 0.8	-86.3	8.2	63.29	-1.39	63.31	358.74	1
PN_9_1_39	00 46 7.30	41 48 8.8	-134.3	6.0	48.06	-12.52	49.67	345.40	1
PN_9_1_38	00 46 8.10	41 51 0.0	-104.3	6.0	50.47	-10.98	51.65	347.72	1
PN_9_3_20	00 46 8.44	42 11 31.5	-81.0	6.0	67.20	0.90	67.21	0.77	1
PN_9_4_35	00 46 9.31	41 55 44.4	-47.5	6.0	54.46	-8.41	55.10	351.22	1
PN_9_3_27	00 46 15.77	42 9 20.8	-80.0	13.5	66.22	-1.47	66.24	358.73	1
PN_9_3_25	00 46 15.93	42 5 35.8	-142.7	6.0	63.19	-3.68	63.29	356.67	1
PN_5_3_35	00 46 18.30	41 31 9.8	-174.9	4.2	35.45	-24.07	42.85	325.82	2
PN_9_4_40	00 46 18.33	41 52 22.5	-140.2	6.0	52.70	-11.73	53.99	347.45	1
PN_9_1_41	00 46 19.13	41 49 42.6	-103.3	8.2	50.62	-13.41	52.36	345.17	1
PN_9_4_41	00 46 26.23	41 55 39.2	-135.2	8.2	56.22	-11.02	57.29	348.91	1

Table A1: Positions and Velocities of Planetary Nebulae.

PN_5_1_12	00 46 31.62	41 12 57.1	-220.9	13.5	22.09	-36.71	42.85	301.04	1
PN_9_3_30	00 46 32.41	42 3 42.1	10.7	5.8	63.43	-7.27	63.84	353.47	2
PN_5_1_11	00 46 35.00	41 12 29.1	-236.3	6.0	22.08	-37.50	43.52	300.50	1
PN_9_1_47	00 46 40.29	41 45 46.0	-134.4	8.2	49.71	-18.91	53.18	339.17	1
PN_9_3_29	00 46 41.49	42 11 57.4	-60.8	13.5	71.12	-3.82	71.22	356.92	1

This paper has been typeset from a TEX/ LATEX file prepared by the author.

NOAO/IRAF V2.11.2EXPORT ch@staru7.livjm.ac.uk Sun 17:20:26 12-Nov-200
[s05M31PNE5_com.0122]: P465   00:42:50.77   +41:17:36.0   22.00 1200. ap:12

Wavelength (angstroms)